UNIVERSIDADE FEDERAL DE PERNAMBUCO
DEPARTAMENTO DE FÍSICA – CCEN
PROGRAMA DE PÓS-GRADUAÇÃO EM FÍSICA

BISMARCK COSTA LIMA

PHOTONIC SPIN GLASS, EXTREME EVENTS AND LÉVY-LIKE BEHAVIOUR IN A CW-PUMPED ERBIUM RANDOM FIBRE LASER

Recife
2019

BISMARCK COSTA LIMA

PHOTONIC SPIN GLASS, EXTREME EVENTS AND LÉVY-LIKE BEHAVIOUR IN A CW-PUMPED ERBIUM RANDOM FIBRE LASER

Tese apresentada ao Programa de Pós-Graduação em Física da Universidade Federal de Pernambuco, como requisito parcial para a obtenção do título de Doutor em Física.

Área de Concentração: Óptica

Orientador: Prof. Anderson Stevens Leônidas Gomes

Recife
2019

Catalogação na fonte
Bibliotecária Arabelly Ascoli CRB4-2068

L732p Lima, Bismarck Costa
Photonic spin glass, extreme events and Lévy-like behaviour in a cw-pumped erbium random fibre laser / Bismarck Costa Lima. – 2019.
87 f.: fig., tab.

Orientador: Anderson Stevens Leônidas Gomes
Tese (Doutorado) – Universidade Federal de Pernambuco. CCEN. Física. Recife, 2019.
Inclui referências.

1. Óptica. 2. Lasers aleatórios. 3. Sistemas complexos. I. Gomes, Anderson Stevens Leônidas (orientador). II. Título.

535.2 CDD (22. ed.) UFPE-FQ 2019-26

BISMARCK COSTA LIMA

PHOTONIC SPIN GLASS, EXTREME EVENTS AND LÉVY-LIKE BEHAVIOUR IN A CW-PUMPED ERBIUM RANDOM FIBRE LASER

Tese apresentada ao Programa de Pós-Graduação em Física da Universidade Federal de Pernambuco, como requisito parcial para a obtenção do título de Doutor Doutora em Física.

Aprovada em: 27/03/2019.

BANCA EXAMINADORA

_____
Prof. Anderson Stevens Leônidas Gomes
Orientador
Universidade Federal de Pernambuco

_____
Prof. Cid Bartolomeu de Araújo
Examinador Interno
Universidade Federal de Pernambuco

_____
Prof. Ernesto Carneiro Pessoa Raposo
Examinador Interno
Universidade Federal de Pernambuco

_____
Prof. André de Lima Moura
Examinador Externo
Universidade Federal de Alagoas

_____
Prof. José Soares de Andrade Júnior
Examinador Externo
Universidade Federal do Ceará

ACKNOWLEDGEMENTS

I am thankful to my family;

I am thankful to my advisor, Anderson Gomes, whose encouragement, guidance and support during my works enabled me to develop an understanding of the subjects.

I am thankful to the Lab colleagues, especially to Pablo, Melissa, Manoel, Ivan, Renato and Mariana for all the help and ideas.

I am thankful to professors Cid Araújo, Leonardo Menezes, Ernesto Raposo, André Moura, Raman Kashyap and José Soares, for positive criticisms which enriched this thesis.

I am thankful to the financial support provided by CAPES and FACEPE, and also CNPq.

I am thankful to the Fabulas Lab from Polytechnic School of Montreal, led by Professor Raman Kashyap, for a fabulous 6 months of sandwich scholarship.

I am thankful to Graziele for accompanying me during this journey.

Lastly, I offer my regards to all of those who supported me during all those years at UFPE.

ABSTRACT

Random lasers (RLs) are photonic systems that emit light amplified by stimulated emission of radiation, (coherent emission) due to multiple scattering of light by a disorder medium inside a gain medium. Since there are no fixed mirrors, the feedback mechanism provided in conventional lasers does not exist here. This role is made by the multiple scattering of light inside the gain medium owing to the presence of scatterers. RL light can present multi-directionality in the emitted beams, multimode character and a complex behaviour due the connection between strong scattering, disorder and gain. RL was first proposed by Letokhov (1968) to occur in any gain material with scattering after a determined volume threshold. Nowadays there are RL in different materials, and one with most potential for applications are RLs that takes the advantages of fibre optics, where laser emission is obtained in conventional or specially designed optical fibres. The complex behaviour of RL light emission has been used to observe statistics phenomena in a well controllable device and performing analogies with statistical mechanics. In this work, we study the statistical properties of the light emitted by an Erbium doped random fibre laser, with a specially designed fibre Bragg grating. In this sense, the feedback mechanism is provided by multiple scattering of light due the intentionally inscribed random phase shifts during the grating writing process. The linewidth reduction and the output intensity as a function of the input pumping power was characterized, showing a typical threshold resembling a conventional laser character. The multimodal behaviour was determined by speckle measurements. Interaction between the laser modes was analysed by the emission spectra performing the analogies to the spin glass theory, considering the laser modes and input pump power analogue to the spin variables and inverse of temperature, respectively. A glassy behaviour was attributed to the Erbium random fibre laser emission by the analysis of the emission spectra. With the definition of the intensities fluctuation order parameter (analogue to the Parisi order parameter), its probability density distribution changes shape, showing that the system goes from a non-correlated regime below threshold to a correlated mode behaviour above the threshold. It is a clear evidence of a photonic paramagnetic to a photonic spin-glass phase transition. From the same experimental data, we characterized the maximum emitted intensity in each spectrum, its connection to the large intensity fluctuation is experimentally studied, and three different regimes on the emit-

ted intensity were observed: Gaussian pre-laser regime, Lévy-like around the threshold and Gaussian laser regime well above the threshold. The large intensity fluctuation also motivated the study of extreme events in this system. We observed the presence of rare events of large intensity fluctuation that well complied with the theoretical prediction. We analysed each sub-set of the maxima intensities emitted, forming a new set of variables. It was observed a good agreement between the Lévy stable distribution and Extreme events statistics, and experimental evidences of connection to the glassy behaviour was experimentally observed. Our results introduce new insights to the understanding random laser emission properties and confirm the use of RL as a photonic platform to study a broad range of physical process, optical amplifiers, sensors and light source to image measurements.

Keywords: Open cavity. Phase-transition. Non-Gaussian. Glassy behaviour.

RESUMO

Lasers aleatórios (LAs) são sistemas fotônicos que emitem luz amplificada por emissão estimulada de radiação (emissão coerente), devido ao múltiplo espalhamento por um meio desordenado em um meio de ganho. Como não existem espelhos fixos, o mecanismo de realimentação fornecido pelos lasers convencionais é inexistente neste sistema. Esse papel é desempenhado pelos espalhadores dentro do meio de ganho. A emissão de LA pode apresentar multidirecionalidade nos feixes emitidos, caráter multímodal e um comportamento complexo devido à conexão entre o espalhamento, desordem e ganho. LA foi proposto pela primeira vez por Letokhov (1968) para ocorrer em qualquer material de ganho com espalhamento após um determinado limiar de volume do meio de ganho. Atualmente existem LAs com diferentes materiais, e um destes com maior potencial para aplicações são os que aproveitam as vantagens de fibras ópticas, onde a emissão do laser é obtida em fibras convencionais ou especialmente projetadas. O comportamento complexo de emissão de luz em LAs tem sido utilizado para observar fenômenos estatísticos de forma controlável e realizar analogias com a mecânica estatística. Neste trabalho, estudamos as propriedades estatísticas da luz emitida por um laser de fibra aleatório dopado com Érbio, com uma rede de Bragg especialmente projetada inscrita na fibra óptica. O mecanismo de retroalimentação é fornecido pelo espalhamento múltiplo da luz devido às mudanças de fase aleatórias inseridas durante o processo de escrita da rede de Bragg, que induz uma variação no índice de refração. A redução da largura de linha e a intensidade de saída em função da potência de bombeamento foi caracterizada, mostrando um comportamento limiar típico de um laser convencional. O caráter multimodal do laser aleatório foi determinado pela técnica de *speckle*. A interação entre os modos deste laser foi analisada pelos espectros de emissão realizando analogias com teoria do vidro de spin, considerando os modos do laser e a potência de bombeamento de entrada análoga às variáveis spin e ao inverso da temperatura, respectivamente. Um comportamento vítreo é atribuído à variação da intensidade da emissão de laser de fibra aleatório de Érbio pela distribuição de densidade de probabilidade do parâmetro de ordem (Parâmetro de Parisi) da flutuação de intensidade ao analisarmos os espectros de emissão, observando a partir do parâmetro de ordem que a flutuação em cada comprimento de onda passam de um regime sem correlação (antes do limiar) para um

regime com correlação. Observa-se claramente uma transição da fase paramagnética fotônica para a fase vidro de spin fotônica. A partir do mesmo conjunto de dados experimentais, analisando os espectros de emissão, caracterizamos o regime estatístico da máxima intensidade emitida em cada espectro, e a sua conexão com flutuação extrema de intensidade é estudada experimentalmente, e três diferentes regimes na intensidade emitida foram observados, regime Gaussiano de pré-laser, regime semelhante à estatística de Lévy em torno do limiar e Gaussiano bem acima do limiar. A flutuação de intensidade também motiva o estudo de Eventos Extremos neste sistema. Observamos a presença de eventos raros de grande flutuação de intensidade em acordo com a previsão teórica. Neste caso, analisamos os máximos de cada subconjunto das intensidades máximas emitidas, formando um novo conjunto de valores. Foi também observada uma conexão entre as estatísticas de distribuição estável de Lévy e de Eventos Extremos, e foram obtidas evidências experimentais adicionais da conexão da estatística de Lévy com o comportamento vítreo. Os nossos resultados introduzem novos conhecimentos para entender as propriedades de emissão de lasers aleatórios e confirmam o seu uso como plataforma para estudo de diversos processos multidisciplinares em física, amplificadores ópticos, sensores e fontes de luz para geração de imagens.

Palavras-chave: Lasers Aleatórios. Sistemas complexos. Estatística de Lévy. Eventos extremos. Vidros de Spin.

LIST OF FIGURES

LIST OF TABLES

CONTENTS

1 LASERS AND RANDOM LASERS

1.1 Lasers

The main process used by a laser device is the amplification by stimulated emission of radiation, followed by oscillation to sustain the gain higher than the losses (1). Stimulated emission occurs when an income photon interacts with the excited medium and stimulate the emission of a second photon. Figure 1 shows the idea of stimulated emission (c) and compares to the absorption (a) and spontaneous emission (b). When a photon of energy hν is resonant with the energy difference of the energy levels, these photons can be absorbed (Figure 1 (a)), promoting the electrons to an excited energy level. The spontaneous emission is a downward energy process (Figure 1 (b)) where an excited atom releases energy by the emission of photons in any direction, without coherence. In the stimulated emission a first photon stimulates the emission of second photon, amplifying the number of existing photons.

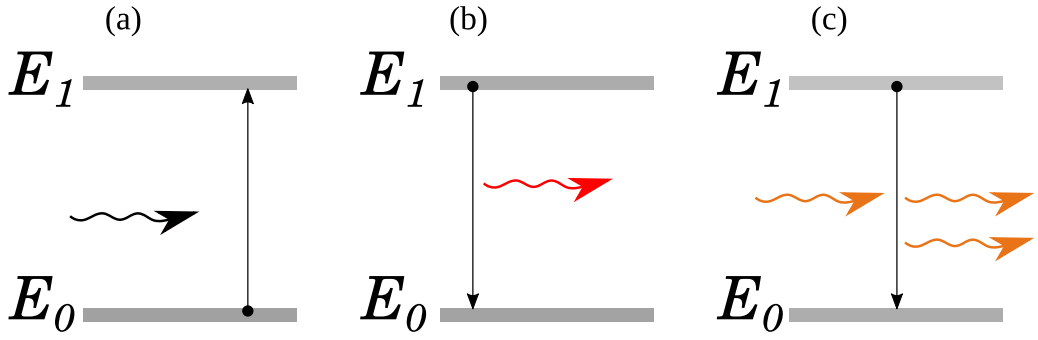

Figure 1 – **Stimulated emission**. The populated and unpopulated energy level used in the optical transition are represented by grey bars, with the energy $E_1 > E_0$. The absorption is represented in (a) where an atom is excited by an upward transition, spontaneous emission in (b) with energy spontaneously emitted, and in (c) a stimulated transition.

The light amplification by stimulated emission is the key of laser devices, together with a feedback mechanism. Essentially, this device is formed by three elements, gain medium, pump mechanism, and an oscillator:

1. A gain medium where the laser process occurs, that can be, a fluorescent material (solid, liquid, gas, etc.). Such material needs to have low surface imper-

fections and low inhomogeneity to avoid light scattering, aiming at reducing the energy loss due to photons leakage;

2. The second element of a laser device is a pump mechanism or an energy source, to induce population inversion in the gain medium, more atoms in an excited state than in ground state. The gain medium needs to be a material with as low scattering as possible otherwise more pump photons are necessary to generate population inversion and then the laser threshold increases;

3. An oscillator, usually two mirrors, to partially trap the light during enough time to be amplified by the active material by stimulated emission, promoting a feedback mechanism. The cavity formed by the mirrors also determines the laser emission modes.

Figure 2 (a) shows a simple scheme of a conventional laser device. The optical pump mechanism is sketched as green laser beams, of frequency ω_p, is on the spectral range of the absorption curve of the gain medium (GM). The amount of energy absorbed by the GM is released by the emission of vibrational energy or by fluorescent process. Photons emitted by the gain medium are partially trapped by the cavity formed by mirrors M_1 and M_2, denominated as a Fabry-Perot cavity. An amount of light bounces back and forth through the GM to be amplified with a gain coefficient β. Another amount leaves the cavity and contribute to the loss. The coefficient α quantify all the loss in the cavity, that are produced by some process, as cavity leakage, scattering, etc. Figure 2 (b) shows a example of transmission of the allowed cavity modes of a Fabry-Perot resonator.

1.1.1 Laser threshold

With the increase of the pump power more photons and gain are generated, until saturation occurs. The gain after one round-trip inside the cavity increases with (1)

$$G_{rt} = r_1 r_2 \exp(2L(\beta - \alpha)), \tag{1.1}$$

where r_1 and r_2 are the reflectivity of the mirrors M_1 and M_2. This equation is valid for a cavity with a gain coefficient β, loss coefficient α, and for a gain material uniformly distributed inside a cavity of length L. Laser emission will occur when in one round-trip,

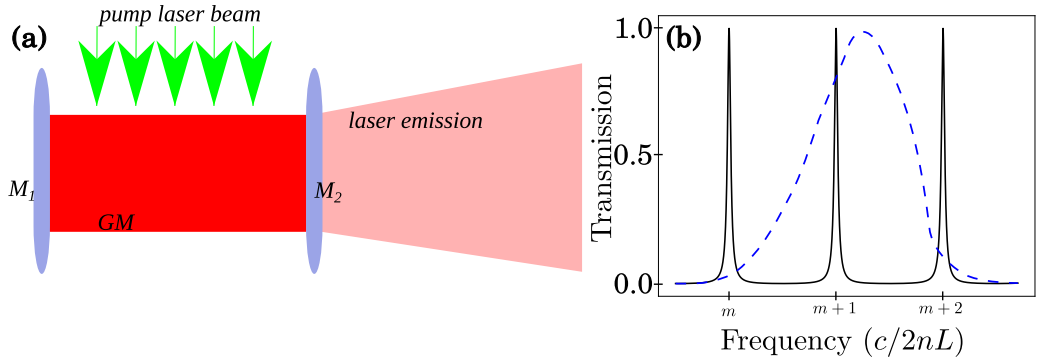

Figure 2 – **A conventional Fabry Perot laser cavity and allowed cavity modes**. (a) Scheme of a laser device formed by two mirrors M_1 and M_2, by the Gain medium (GM) and a pump energy source sketched as a green laser (down arrows). The laser beam output is through the mirror with lower reflectivity. Allowed cavity modes of a Fabry-Perot resonator with reflectivity of the mirror $r_1 = 0.9999$ and $r_2 = 0.8r_1$. In this case the mode $(m+1)$ do the best overlap with the hypothetically fluorescence emission curve, represented by the dashed blue lines. Above the threshold the laser emission is more like probable to occur at this frequency.

the amount of energy that bounces the cavity exceeds the amount of loss $\beta > \alpha$, and the gain is $G_{rt} \geq 1$.

The Fabry-Perot *"consisted of two closely spaced and highly reflecting mirrors, with mirrors surfaces adjusted to be as flat and parallel to each other as possible. [...], such Fabry-Perot interferometer or etalon can have sharp resonances or transmission passband at discrete optical frequencies"* (Siegman p. 409 (1)). Longitudinal transmission cavity modes have frequencies

$$\nu_m = m\frac{c}{2nL},\ m = 1, 2, 3, \cdots, \tag{1.2}$$

with a uniform refractive index n in the whole cavity.

After the gain surpasses the losses, the curve of the emitted power versus input power increases (usually) linearly, the threshold input power is represented in Figure 3 as P_{th}. Simultaneously, a spectral narrowing occurs.

The emitted laser frequency, is balanced by the frequency curve of the fluorescent emitted light and the allowed mode frequencies of the cavity ν_m, as sketched in Figure 2 (b). The mode that matches with the gain curve of the amplifying medium will be favoured and can determine the laser emission frequency (wavelength). Some other mechanism can change the emission, but their study is beyond the purpose of

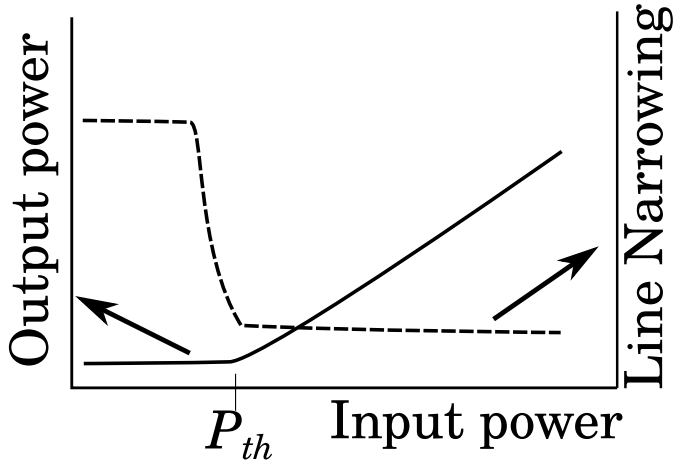

Figure 3 – **Laser threshold**. Output versus input power picture of laser emission (continuous curve) and spectral narrowing (dashed curve), the changes on the curve slope is an evidence of laser threshold.

this work and can be found in Reference (1).

The characteristic of the light emitted by lasers varies greatly. Usually the emission is directional and has a high spatial coherence that can results in a high beam quality, and high intensity. In the temporal scenario, the electric field of the electromagnetic wave oscillates in phase providing high temporal coherence and a single frequency laser operation can be obtained. In some cases, spatial coherence can be a disadvantage of the conventional lasers. For example, the well known grainy interference pattern (2), formed by the interference of wave fronts of same frequency but out of phase and with different amplitudes, the so-called speckle pattern, can be harmful to laser images applications. However, they can be used to understand the properties of a scattering material or track biological system (2, 3).

1.1.2 Scattering

Light scattering often happens in our daily lives, usually when light propagates and hit small particles (compared to the wavelength of the light) or, pass through a medium with different refractive index values. Atmospheric phenomena arises from these effect such as the colour of the sky and fog (4, 5, 6, 7). The scatter can be due to molecules, impurities or inhomogeneity in the medium refractive index. Specifically, the blue colour of the sky is explained by the Rayleigh scattering, where the intensity of the scattered light (I_s) is inversely proportional to the wavelength (λ_I) of the incident

photons ($I_s \propto 1/\lambda_I^4$) (7).

The scattering of light is classified as elastic and inelastic. In the first category are included scattering processes that occur with no change in the frequency of the incident wave, where the Mie and Rayleigh scattering are included. The first is related to phenomenon when the electromagnetic wave is scattered by particles with dimensions of the order of the wavelength of incident light. Rayleigh scattering occurs for particles with dimensions much smaller than the wavelength of the electromagnetic wave.

In the class of inelastic scattering are processes that has a change in the frequency of the incident photon, loosing or gaining energy. The Raman scattering is an example, whereby an incident electromagnetic wave of frequency ω_I in a molecular system is scattered. The scattered wave frequency is $\omega_S = \omega_I \pm \omega_{VE}$, where the change of the incident frequency is determined by the material vibrational energy, that is proportional to the vibrational frequency ω_{VE}, In the case where incident light loses energy (smaller frequency, higher wavelength), Raman Stokes nomenclature is used, just similar as is used in the fluorescent stokes emission nomenclature, even though they are different processes.

Conversely, when energy is absorbed by the incident wave in the scattering process an anti-stokes Raman scattering occur. The Brillouin scattering class is another inelastic process. It is similar to the Raman scattering, but the energy change in the scattered photons are due to the presence of large number of low energy phonons, or acoustic phonons.

1.2 Random Lasers

Leaving behind systems where light scattering is detrimental, there is at least one system where this effect is desired. Known as random laser (RL), they are systems that uses highly disordered medium to scatter the emitted stimulated photons from a gain material or the gain material and scatter are the same, with feedback being provided by multiple scattering of light inside the gain medium. The word **random** arises because the major role that determine the feedback process is the random path travelled by light, forced by randomly distributed scatters centres (8).

A conventional laser cavity is usually formed by well-defined mirrors, that will provide the properties of the emitted light. But, RL do not have such typical cavity

with the characteristics $c/2L$ modes. Instead of it, the scatter centres play the role of mirrors, similar to randomly distributed cavities. To provide such scattering effect in RL, small particles can be used (9), fluctuation in the medium refractive index (10), natural structures present in biological systems (11), crystal powder (8), etc. The RL scatterers can be embedded in the gain medium, as a laser dye with scattering particles. Or the gain medium can be both, the active and the scattering material, for example, as occur in a semiconductor powder (12).

The first proposal of light amplification in a scattering material was made, theoretically, by V. S. Letokhov in 1968 (13) after a sequence of works of R. V. Ambartsumyan and the Nobel laureate Basov (14, 15, 16, 17). Since the first clear experimental demonstration, that was done by N. M Lawandy et al. (9), a great number of works has been developed. Nowadays there are random lasers in a great amount of materials, in different geometries, in three-dimensional bulk (9, 18, 19) and two-dimensional layers material (11, 20, 21). Exploiting the optical fibres geometries had led to a quasi-one-dimensional random laser (10, 22, 23).

Several RL applications arises as in fundamental and applied physics. The open cavity characteristic of multimodal RL and strong scattering are favourable to multimode interaction. RL has complex behaviour that makes it a photonics platform for statistical physics studies (24). The low spatial coherence of RL provides a speckle free laser that can be direct used to acquire speckle-free high-quality images (25). In this section, the introductory characteristics of random laser are presented.

1.2.1 Lasers with non-resonant feedback

The idea to use a laser system with non-resonant feedback[1] is old and is dated from 1966. R. V. Ambartsumyan published a work that demonstrated a laser with two ruby crystal as gain medium (15). The feedback mechanism was provided by a mirror with reflection of 70% and a scatter material, an aluminium plate surface of magnesium oxide film sputtered on, or by a volume material with sulphur particles. The experimental setup used by Ambartsumyan is drawn on Figure 4, (a) represents the scatter material, (b) and (c) is the gain medium and (d) a mirror, and the collection set up is made by filter (e) a photo detector and (f) and oscilloscope (g). The threshold value

[1] Random Lasers were only called as such after 1995. Until then, different nomenclatures were used. For the sake of clarity, we will call it a random laser from the beginning.

was dependent of the separation distance between the gain and scatter material and was independent of the inclination angle of the scatter medium, showing the relevance of the amount of photons that are backscattered for the laser emission.

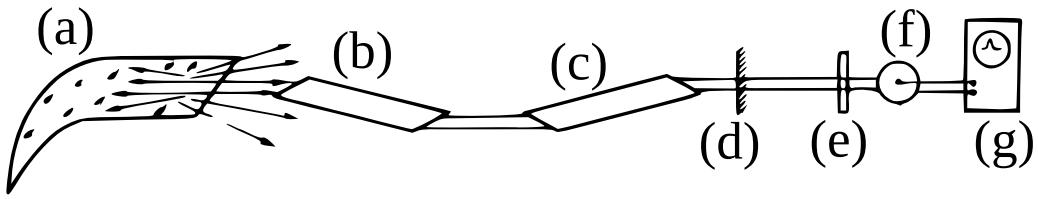

Figure 4 – **Experimental setup used by R. V. Ambartsumyan in 1966**. Scatter medium provided the feedback (a). The gain medium is composed of two ruby crystals (b) and (c). Output mirror (d). Filter (e), photo-detector (f) and an oscilloscope (g). Figure adapted from Reference (15).

Above the threshold, the emission fluctuations were similar for a laser. The fact that they used a mirror does not lead to the laser modes exhibit resonant properties but decrease the laser threshold in more than two orders of magnitude. This non-resonant feedback laser did not show the typical frequencies $c/2L$ of resonant lasers. The modes were coupled, and the frequency of the active medium determined the laser frequencies. They also observed low spatial coherence and unusual linewidth reduction dynamics, and the intensity distribution in the laser image recorded was more uniform in the non-resonant feedback than when compared to the resonant feedback case. Such characteristic is also similar to the current random laser system, which was first predicted one year later.

1.2.2 Negative absorption in a scattering medium

Vladilen S. Letokhov theoretically showed that it is possible to generate laser emission from a scattering medium with negative resonance absorption (i.e., gain), and he called such material a photonic bomb (13). To derive the proper equation, the author started from the diffusion equation of photons, analogue to neutron's diffusion equation (8)

$$\frac{\partial \vec{W}(\vec{r},t)}{\partial t} = D\nabla^2 \vec{W}(\vec{r},t) + \frac{v}{l_g}\vec{W}(\vec{r},t) \tag{1.3}$$

where $\vec{W}(\vec{r},t)$ is the photon energy density, v is the velocity of the light inside the scattering medium, l_g is the gain length (negative absorption), and the diffusion coefficient is $D = vl_t/3$, where l_t is the transport mean free path. The general solution to Equation

1.3, for the case of a homogeneous pump was written as,

$$\vec{W}(\vec{r},t) = \sum_{n}^{\infty} a_n \Psi_n(\vec{r}) \exp\left[-t\left(DB_n^2 - \frac{v}{l_g}\right)\right] \tag{1.4}$$

where a_n is a constant determined by the boundary conditions, $\Psi = 0$ at the boundaries of the scattering medium, Ψ_n and B_n are eigenfunctions and eigenvalues of the Equation 1.5, where, $B_n = 2\pi n/L$ for a sphere of radius $L/2$.

$$\nabla^2 \Psi_n(\vec{r}) + B_n^2 \Psi_n(\vec{r}) = 0 \tag{1.5}$$

Analysing the solution 1.4 of the Equation 1.3, there is a determined length of the scattering medium where the eigenvalues B_n goes smaller enough to the gain surpass the absorption. This threshold values occur when the Equation 1.4 changes from an exponential decay to an exponential increase, this condition is defined by

$$DB_n^2 - v/l_g = 0. \tag{1.6}$$

When $DB_n^2 < v/l_g$, the system is dominated by negative absorption, and the threshold values is at $DB_n^2 = v/l_g$. For a medium of dimension L, and for the lowest eigenvalue the condition for threshold is $L \sim \sqrt{(l_t l_g)/3}$ (8), which determines the critical volume to occur negative absorption, the proportionality factor is determined by the shape of the scattering medium.

1.2.3 Modes in random laser

Orthogonal solutions of light propagation give the concept of modes with shape determined by the diffraction and boundary conditions (26). The open cavity and strong scattering characteristics do not make RL modeless. The propagation of light here is provided by the long-lived modes related to the electromagnetic expansion in term of spatial modes eigenvector $\mathbf{E}(\mathbf{r})$. Indeed, such properties are very propitious to multimode behaviour. Instead of $c/2L$ characteristics of Fabry-Perrot resonators modes, the RL lasers modes are determined by the path travelled by the light scattered in the active material. Some authors (24, 27, 12, 28) initially proposed two different RL regimes, resonant (coherent) and intensity feedback (incoherent). In the coherent feedback, closed loops are responsible to narrow linewidth peaks emissions by interference effects of the travelling wave, which is a resonant feedback mechanism, these peaks show typical characteristic of laser light, such as Poisson count statistics. In a scattering medium

light can return to the starting point and all photons that are backscattered can suffer by interference effect. The modes that have constructive interference effects, with a phase delay $2\pi n,\ n = 1, 2, 3...$, and the gain surpass the loss will have laser emission (8).

The non-resonant or intensity feedback mechanism is provided by waves that propagates by open paths and interference effects are not observed. However, even without the presence of narrow linewidth peaks or with a narrow smooth spectrum with modes averaged out the emission is multimode, e.g., coherent effects are present in the system even whereas the spectra are smooth. Then, the inability to observe the narrowing linewidth peaks in random laser (multimode behaviour) is owing to the lack of experimental setting (24). The ideal conditions to observe ultra-narrow peaks is using excitation with low pulse duration (ps) (12, 29) and single-shoot observation (24).

1.3 Bulk Random Laser

Random laser can be defined as devices where the feedback mechanism and the laser process are determined by multiple scattering of light (24). RL has typical length scales to describe the scattering process (27):

- The scattering mean free path $l_s = (n_s\sigma_s)^{-1}$ is defined as the distance between two consecutive scattering events, in a medium with the density of scatter n_s, and averaged scattering cross section σ_s;
- The transport length $l_t = (l_s)/(1 - \langle\cos\theta\rangle)$ is defined as the average distance the wave travels before its direction of propagation is randomized ($\langle\cos\theta\rangle$ is the average cosine of the scattering angle);
- Amplification length l_{amp} is defined as the root-mean-square average distance travelled between the start and end point for path of length l_g, when the amplification length becomes smaller than the typical distance travelled by photons to leave the sample the laser emission occurs;
- l_g is the gain length, the distance travelled until the intensity is amplified by a factor of e.
- Other characteristics are the size of the random medium L and the volume.

RL light transport operate in different regimes, and analogue definitions applied to electron transport can be used here. The ballistic regime occurs when the dimensions L of the scattering medium is less or equal to the scattering mean free path $L \leq l_s$. In this case, the photons can propagate through the whole material without any scatter event, and the feedback can be provided by backscattering reflection. The diffuse transport regime occurs when the wavelength that propagates in the scatter material is $\lambda \leq l_s \leq L$. And the localization regime is when the effective wave vector in the random media k is related to $kl_s \cong 1$. RL feedback is provided only by the random scattering of light in a high scattering active medium, and can be obtained in many ways. The most common are nano-particles colloidal suspension (9), powder crystal (12) and porous materials (30). Those scattering can be inherent to the material or artificially made.

1.3.1 Random laser material and emission

A material for RL must provide a medium where the light can suffer enough elastic scattering before goes out, e.g. the amplification length must be smaller than the sample size. The l_t need to be at least smaller than the sample dimensions. A large value of l means a weak scattering regime. The angular spectral pattern of the random laser emission is dependent on the scattering strength.

For low l_s values, the emitted spectra as a function of collected angle maintains its shape, and for high values even the wavelength of the peak intensity can change for different collected angles (31).

The relatively easy production makes a wide number of materials being exploited for RL manufacture, as liquid dyes (9, 19), polymers (32), powder crystal (18, 12), bio-materials (11, 21), glasses where changes in the refractive index plays the role of scatter (23), etc. A review of each material is far beyond the purpose of this thesis. Reference (30) are review most of the published works until 2015.

As already mentioned, the emission emerging from bulk RL are generally multidirectional. Because of the random nature of the path travelled by photons in the random medium, taking control of the emitted direction of this system is not an easy task, although work in this direction has been reported (33, 34). In the diffusive scattering regime, for example, using spherical SiO_2 scatters in Rhodamine 6G dye, most of

the RL light is emitted in the backward direction, the intensity emission decreases for large angles measured in relation of the pump beam because of the re-absorption by unexcited dye molecules (31).

The association of strongly scattering medium and gain competition, have led RL to exhibit complex behaviour in the intensity emitted spectra (24). Large fluctuation in the emitted intensity of the RL systems at and above the threshold value is observed (28). The main reason for such effect at the threshold are gain competition, lucky photons that almost retain all the gain, achieving amplification with different path length, and the fluctuation in the path length (28, 35, 29, 8, 36). The multimode characteristic of random laser creates a wide energy landscape where the system can reach (37, 38). At every time that a spectrum is collected, it can exhibit a different shape, observing intensity fluctuation as result of mode interaction. A detailed description of these characteristics will be present in the chapter 3 when non-Gaussian and extreme events statistic of the emitted intensity of RL in optical fibres are presented, and in the chapter 2 when the photonic analogue of spin glasses system emerged from multimode interaction is studied.

Two examples of bulk materials used for 3D RLs are rare-earth doped powders and colloids based on laser dyes, as briefly reviewed below.

1.3.2 Powder random laser

Work based on powder materials shown characteristics of laser like emission, spectral narrowing and slope change in the emitted intensity versus the pump power (8). But in such systems with micro-particles, was difficult to say, when the feedback mechanism was provided by multiple scattering of light, or by total internal reflection inside the powder particles.

V. M. Markushev *et al.* (39) did the first experimental study of laser emission in a scatter material, the sample was a powder phosphor of $Na_5La_{1-x}Nd_x(MoO_4)_4$, formed by micro-particles with dimensions varied between 1 μm and 10 μm, excited by nanosecond tunable Rhodamine 6G laser. The authors observed a clear threshold behaviour, characterized by strong reduction of emission pulse lifetime (at $\lambda \approx 1066$ nm), a reduction in the spectra linewidth and a huge emission intensity increase. Worth noticing is that at the Markushev's paper was observed that laser emission occurs at

the point where the spontaneous emission was maximum.

Random laser emission was demonstrated in Nd^3 doped YBO nano-crystals, of centre symmetric and hexagonal structure (40). With an excitation pumping laser operating at 806 nm, the RL emission occur at 1056 nm. A photonic spin-glass transition was observed in this system, and a suppression of the glass behaviour at high pump power were finding (40).

Self-second-harmonic generation and self-sum-frequency using $Nd_xY_{1.00-x}Al_3(BO_3)_4$ nano-crystal powder, with tunable laser emission by varying the Nd concentration is also reported in powder RL (41).

1.3.3 Dye colloidal random laser

Dye lasers provide wide spectrum range lasers and are easily tunable, in liquids or solid state materials. The first unambiguous demonstration of random laser was made in a dye colloidal suspension of TiO_2 nanoparticles in Rhodamine dye (9), where Lawandy et al. proposed a system where the gain medium and the scattering materials are distinct (9), differently for the micro-particles case where doubt on feedback were present. Using a colloidal solution of TiO_2 nano-particles embedded in Rhodamine 640 dye in methanol, pumped by 532 nm radiation of a frequency doubled Nd:YAG laser, they observed that such colloid has a typical threshold value. The slope of the intensity emitted as a function of the pump power change, emitted intensity grew linearly after the threshold and the spectral full width at the half maximum (FWHM) decreases. The observed narrowing linewidth from 80 nm to 5 nm, was dependent of the transport length (9, 42, 43).

This work was a trigger to the development of works to study the basic processes behind the random laser materials, including the role of scattering concentration and other characteristics in such laser process. Rhodamine dyes are widely used compound for dye RL, as it has a broad emission in the visible spectra and depending on the solvent medium and, owing to the high absorption, this dye material can be easily excited by the second harmonic of a Nd:YAG laser.

Controlling the scattering and dye concentration, is possible to observe a linewidth reduction of the emission spectra as the pump energy increases, and is followed by a high enhancement in the emitted peak intensity. This process is different from the ef-

fect of amplified spontaneous emission, where spontaneous emitted light is amplified when passes through a region with excited dye molecules. As was shown by Lawandy in 1994 (9), the emission linewidth reduces with the reduction of the transport length l_t, and the RL emitted pulse duration is almost ten times less than in a pure dye compound.

Other way to use dye compound are in porous material, to make a solid-state dye RL. The Rhodamine can be infiltrated in the alumina ceramic with porous of micrometers dimensions. Scattering mechanism is provided by the porous structure (44). The first experimental demonstration of a random fibre laser was also performed with dye gain medium inserted into a hollow optical fibre with TiO_2 scattering particles (22).

Dye colloidal random laser, also called laser paint, is usually formed by nano-particles embedded in a dissolved dye. This material also suffers from emission instability due the nano-particles precipitation, drastically reducing the emission intensity after few hundreds pump pulse, but with the use of specially designed nano-particles, as in Reference (45), a dye random laser that maintain stable even after 80,000 pump pulses was obtained, a practically static scatter medium. Therefore, it provided the opportunity to observe the spin glass transition in dye RL. Such effect is studied in the context of random fibre laser in the next chapter.

1.4 Random fibre laser

In Reference (22), a hollow core optical fibre was filled with a dye Rhodamine colloidal suspension with scattering nano particles. Exciting the molecules with a transverse pumping the authors observed laser emission due the scattering gain medium. That was the first experimental demonstration of a random fibre laser (RFL), which was more efficient than their bulk similar device. Presently, the most common way to generate RFL is using the Raman gain in optical fibre, which were first demonstrated by Churkin et al. (46), and reviewed by Turitsyn et al. (10). Spontaneous Raman emission is a process that resembles fluorescence, but are distinct effects (47). Likewise, the stimulated Raman scattering is similar to the stimulated emission, but it occurs only after a critical pump power. The stimulated scattering process arises when an intense excitation light generates strong stokes light field with n photons. If the stokes waves interacts with the next excitation photon in the media, is possible to generate a new one

resulting in $n + 1$ Raman stokes photons, in a fast process.

In a laser system, it is necessary to store enough energy to amplify the subsequent photons, and it is made by the population inversion of the gain medium. However, the stored energy in the Raman scattering is gone after the pulse ends. If the pump mechanism is not strong and fast, stimulated Raman effect will not occur, so the fundamental mechanism to Raman laser will not be present. Strong scattering medium takes the advantages of enhances the possibility of interaction of the emitted waves and incident waves with the matter (31, 36, 48). Turitsyn et al. in 2010 demonstrated for the first time a Raman random laser (23). The Rayleigh scattering due fluctuations in the refractive index of long fibres was used as the feedback mechanism. Raman laser emission was latter demonstrated in different optical fibres, as in short fibres with longs fibre Bragg gratings (49).

In bulk material, from the random walk view, has a completely different dynamic from low dimensional systems. Raman RL in bulk was showen by Hokr et al. (48) 4 years later of the work of Turitsyn. The authors used as gain media a strong scatter Raman active material in the visible spectrum. The disordered $BaSO_4$ powder nanostructure was pumped by a 532 nm laser of 50 ps pulse duration. After a determined critical volume, the stimulated Raman scattering dominates, and linewidth reduction of the Raman scattering was measured. This work opened a whole host of applications, as the Raman scattering material are commonly system. For example, if in an unknown powder material is irradiated by a strong laser pulse, another strong laser pulse can be generated, and makes it detected at distances (50). Such process can be used in detection of chemical material composition using the Stokes shifted values.

Random laser is an attractive system with a wide range of applications and basic studies. The research on RL system are still opens. A better understand of light localization process and light diffusion in random media is still an important task to control the emission properties of Random Laser. Random fibre lasers are a very convenient platform to study RL properties. It has control on directionality of the random laser, can work in both CW and pulsed regime and can operate in the Anderson localization regime (10). Also, Raman fibre laser can open the possibility to obtain emission power of hundreds of watts (51). The use of fibre Bragg grating as scatter medium allow Raman random laser emission in short length fibre optics (52).

1.4.1 Fibre Bragg Grating

A common problem of laser where the feedback is provided by scattering material is the non-uniform distribution of the gain, as not only the spontaneous emission, also the pump beam is affected by scatters. Then, the goal is obtaining scatterers that acts only on the emitted light of the gain medium. A smart way to provide this kind of material, that non-longer can directly affect the pump light, is using fibre Bragg grating (FBG), which is permanently inscribed by modulation of the refractive index of the optical fibre core.

The orthogonal modes that propagates in a waveguide with a grating have forward and backward components written as (53):

$$\left[\frac{\partial A_\nu}{\partial z}\exp[i(\omega t-\beta_\nu z)]+c.c.\right]-\left[\frac{\partial B_\nu}{\partial z}\exp[i(\omega t+\beta_\nu z)]+cc\right]= \frac{i}{2\omega}\int_{-\infty}^{\infty}\int_{-\infty}^{\infty}\left(\frac{\partial^2}{\partial^2 t^2}dxdyP_{grating,t}a^*_{\mu,\nu t}\right) \tag{1.7}$$

where A_ν and B_ν are the forward and backward propagation modes, respectively a is the radial transverse field distribution of the guided modes, $P_{grating}$ is the perturbation on the polarization response of the dielectric media, that for a periodic modulation is (53),

$$P_{grating}=2n\epsilon_0\left[1+\frac{\Delta n}{2}\left(e^{i[(2\pi N/\Lambda)+\phi(z)]}+c.c.\right)\right]E_\mu \tag{1.8}$$

Considering this perturbation and coupling between the forward and their identical backward propagation mode, e.g., the coupling between the input wave and reflected signal, the new equation for the forward and backward waves, as derived in Reference (53) chapter 4.3, as:

$$\frac{dI}{dz}+i\left[\kappa_{dc}+\frac{1}{2}(\Delta\beta)\right]I=-i\kappa^*_{dc}O/2 \tag{1.9}$$

$$\frac{dO}{dz}-i\left[\kappa_{dc}+\frac{1}{2}(\Delta\beta)\right]O=i\kappa_{dc}I/2 \tag{1.10}$$

where $\Delta\beta=\beta_\mu\pm\beta_\nu-2\pi N/\Lambda$ is the phase matching condition between two different modes propagating in a perturbed waveguide with N modulations with period Λ, it can be interpreted as parameter that determines how fast the power exchange between the modes decreases (53). The input wave is $I=A_\nu e^{-\frac{1}{2}[\Delta\beta z-\phi(z)]}$ and the reflected signal $O=B_\nu e^{\frac{1}{2}[\Delta\beta z-\phi(z)]}$, κ_{dc} influences the mode propagation due the average changes in

the refractive index modulations. The phase $\phi = constant$ in Equation 1.8 for a uniform FBG and reflection amplitude signal, in a waveguide of modulation length L, can be written as:

$$\rho = \frac{(\kappa_{dc}/2)\sinh(\varphi L)}{\delta \sinh(\varphi L) - i\varphi cosh(\varphi L)} \tag{1.11}$$

where the detuning parameter as a function of the input wavelength λ is $\delta = \kappa_{dc} + \frac{\Delta\beta}{2}$, when the detuning $\delta = 0$, the forward wave has a maximum coupling with the backward wave signal, e.g., the reflectivity is maximum. $\varphi = \sqrt{|\kappa_{dc}|^2 - \delta^2}$ and $\Delta\beta = (4\pi n_{eff}(\lambda_B - \lambda))/(\lambda)$. The peak reflectivity will occur at the Bragg wavelength $\lambda_B = 2n_{eff}\Lambda$. A scheme of the transmitted and reflect light by an FBG is in Figure 5.

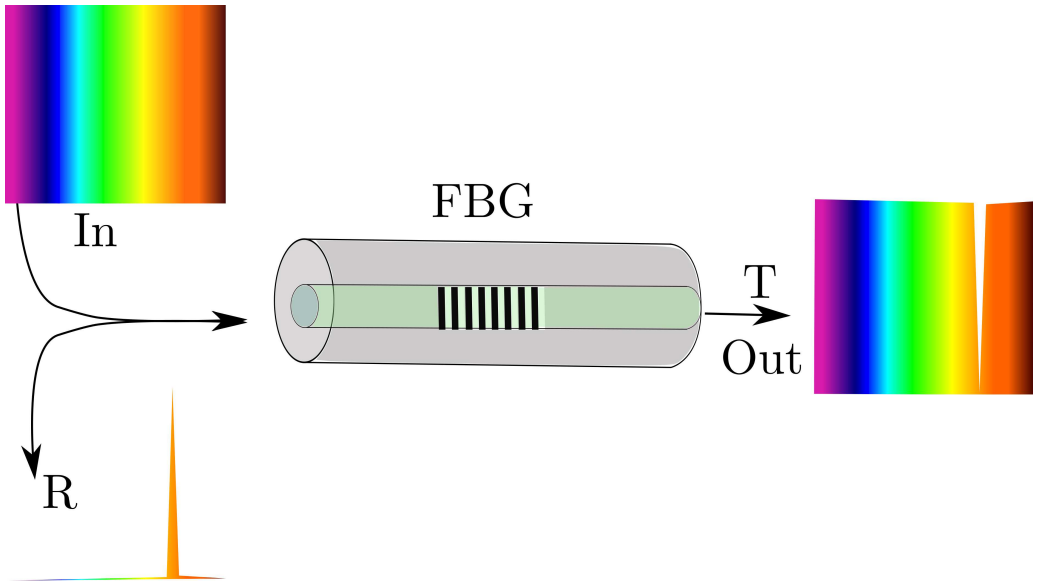

Figure 5 – **Sketch of light transmission and reflection of an FBG**. When a broadband spectrum enters the waveguide with an FBG, the reflected spectrum has a peak at the Bragg wavelength, with a very narrow linewidth ($\Delta\lambda \approx \frac{\lambda^2}{2n_{eff}L}$). De deep in the transmission signal is also present.

FBG can be obtained using a photosensitive optical fibre, e.g. a silica fibre with the core doped with Ge or Ge-Sn, and so by hydrogenation of the fibre (53). This dopant material makes the core refractive index sensible to UV-light, when it is exposed to a UV radiation interference pattern, the refractive index increases in the bright interference fringes. Different methods can be applied to fabricate FBG (53), the simplest way is using a phase mask to induce a UV interference pattern on the fibre, actually, this makes a copy of the phase mask patter in the fibre core refractive index modulation.

1.4.2 Phase shift in a fibre Bragg grating

In a matrix form, a uniform FBG of length L with the input signal I normalized to 1, has reflected signal at the output $-L/2$ and transmitted signal at the output $L/2$ modelled as (53, 54) :

$$\begin{bmatrix} 1 \\ S(-L/2) \end{bmatrix} = \begin{bmatrix} T_{11} & T_{12} \\ T_{21} & T_{22} \end{bmatrix} \begin{bmatrix} R(L/2) \\ 0 \end{bmatrix} \tag{1.12}$$

where $T_{11} = \cos(\alpha L) + \frac{i\sin(\alpha L)\delta}{\alpha}$, $T_{22} = \cos(\alpha L) - \frac{i\sin(\alpha L)\delta}{\alpha}$, $T_{12} = \frac{-i\kappa_{dc}\sin(\alpha L)\delta}{2\alpha}$, $T_{12} = \frac{i\kappa_{dc}\sin(\alpha L)\delta}{2\alpha}$. Some phase shift in an uniform FBG can be induced. It can be by splitting the uniform FBG in parts after and before the phase shift positions, with matrix T_a and T_b, and inserting the phase shift matrix T_{fs} between them. Such that the total matrix $T = T_a T_{fs} T_b$. For a system with n uniform FBG segments, separated by phase shift, the matrix T is written as:

$$T = T_2 T_{fs} T_1$$

$$T = T_3 T_{fs2} T_2 T_{fs} T_1$$

$$\vdots$$

$$T = T_n T_{fs(n-1)} T_{n-1} \cdots T_3 T_{fs2} T_2 T_{fs} T_1 \tag{1.13}$$

The expected effect by the insertion of different phase shifts in an FBG are shown in Figure 6. While the uniform modulation in the refractive index couple only λ_B (Fig. 6 (a)), the insertion of a phase shifts provides more coupling between the forward and backward waves 6 (b-c).

1.4.3 Random laser based on random fibre Bragg grating

Lizárraga et al (55), wrote several FBG with different lengths in a fibre. The FBGs were separated by different distances, making a chain of random distributed FBG that the distance between them will act like scatter. They demonstrate random laser, with emission spectra dependent on the number of written gratings. However, this technique allows the insertion of only few FBGs, thus limiting the number of scatters by the fibre length.

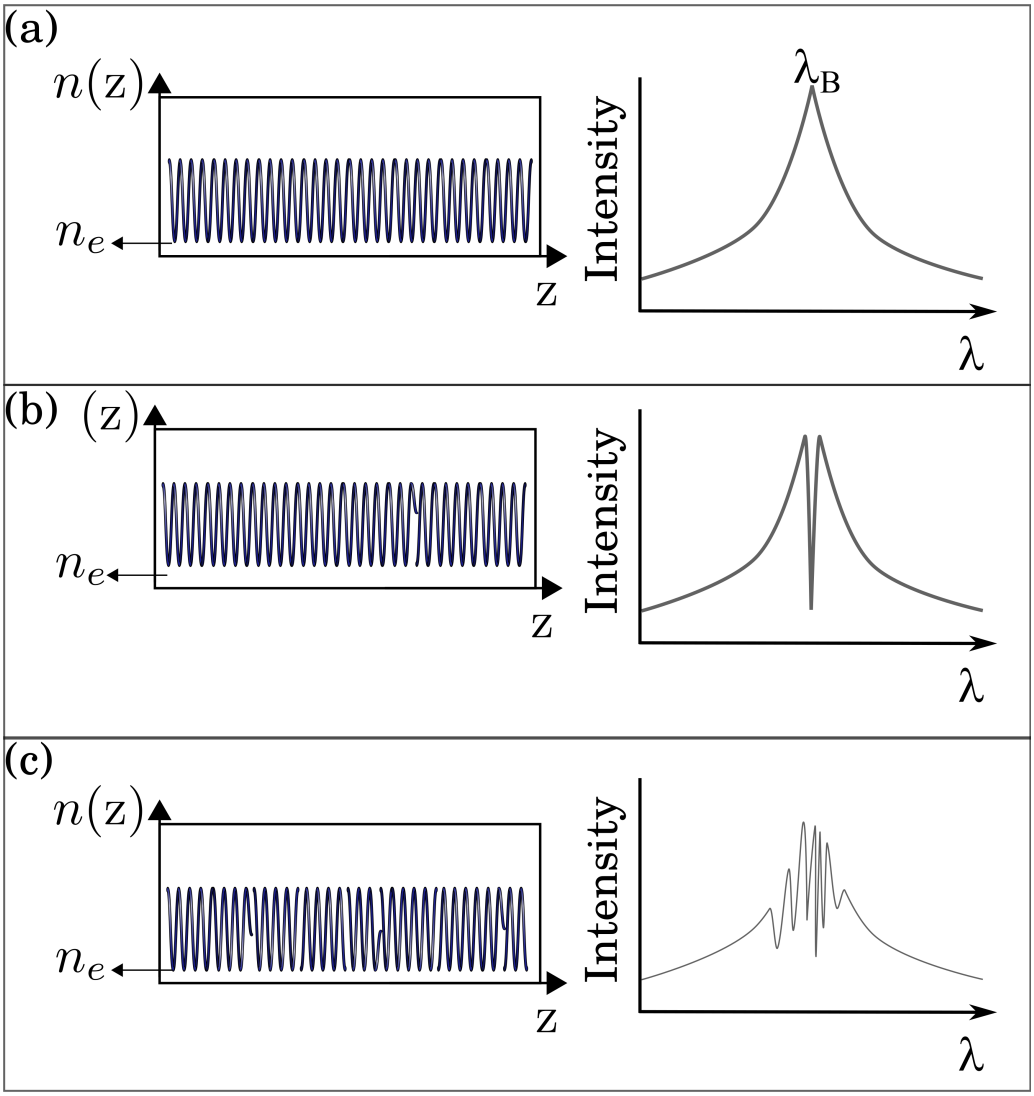

Figure 6 – **Phase shift effect in the backward wave propagation in FBGs**. Sketched modulation of refractive index and expected reflectivity for a uniform FBG (a), an FBG with a unique phase shift (b) and FBG with some phase shift (c).

1.4.4 Fabrication procedure of random fibre Bragg grating

In 2008 M. Gagné and co-works (56) published a novel fibre Bragg grating fabrication method. The main goal of the author was to develop a method to write long FBG. The method consists of an interferometer as sketched in the Figure 7.

A UV beam incident over a phase mask has the diffraction orders ± 1 incident over the optical fibre. Phase modulator (PM) are used to synchronize the fringe pattern with the optical fibre movement, e.g., while the optical fibre is pulled the UV interference pattern moving with the fibre, and a periodic and long FBG is inscribed into the fibre core. When the authors measured the transmitted and reflected spectrum, was

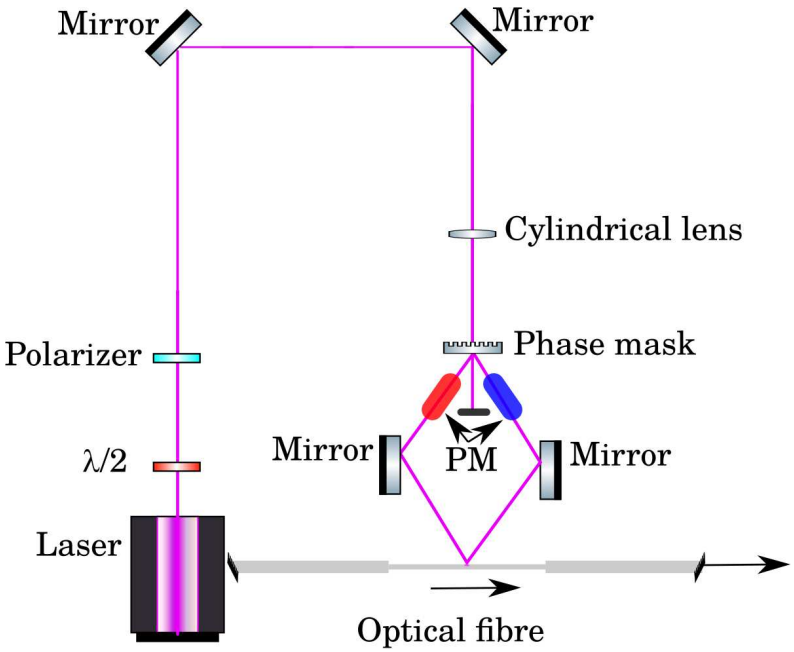

Figure 7 – **Random phase shift FBG fabrication**. Scheme of the experimental setup that can be used to fabricate FBG. A UV laser beam is used to induce a refractive index change in the optical fibre core, a $\lambda/2$ and a polarize is set to control the laser intensity that is focused by a cylindrical lens over a phase mask. A continuous movement of the phase mask holder moves the fringes of the interference patter, and a different approach with two phase modulation (PM) can be used for it. The interference patter moves synchronized with fibre movement. The vibration on the optical fibre caused by friction with the fibre holders when is pulled, introduces random phase shift in random position into the FBG. The fringes patter is generated by fourth harmonic (266 nm) of the Spectra-Physics Q-switched Nd:YLF laser operating at 1064 nm, and set to 25 kHz with a UV average power of 400 mW.

observed a lot of narrow peaks signalling the presence of many phase shifts. It occurs because the method used to translate the optical fibre generates friction with the fibre holders, and it shakes the optical fibre generating misalignment (57). It introduces phase shift into the FBG, in true random position with random intensity. The transmission and reflection spectra of such grating are shown in Figure 8. The large number of scatters can be observed by the presence of large number of peaks due the phase shifts.

1.4.5 Erbium doped random fibre laser

Gagné *et al.* (49) used the aforementioned kind of random fibre Bragg grating to demonstrate a random fibre laser where the scattering process are generated by

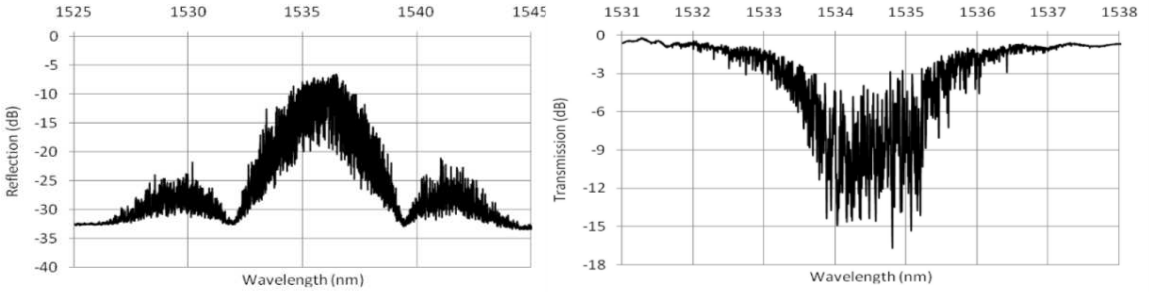

Figure 8 – **Transmission and reflection spectra of a 30 cm FBG with random phase shifts, adapted from Reference (49)**. In left side reflection spectrum measured with resolution of 3 pm, and transmission spectrum on the right side. Many individual peaks was observed due the large number of phase shifts inserted during the fabrication process.

random phase shifts into a unique FBG. The random FBG of 30 cm (or 20 cm) length was written in an Erbium doped optical fibre, the phase shifts inserted in the fabrication process play the role of many scatters, obtaining a device with scattering and gain. After injection of a pump laser beam (980 nm or 1480 nm) laser emission with low threshold value of 3 mW and narrow linewidth, ≈0.5 pm, was observed. The emission power versus input pump power measurements is shown on the left side of Figure 9, where the power emission characteristic of the two devices (20 cm or 30 cm long random FBG) as a function of the pump power is explored using a 980 nm or 1480 nm lasers. The laser emission occurs when the device have length L larger than the localization length ($L > 5$ cm).

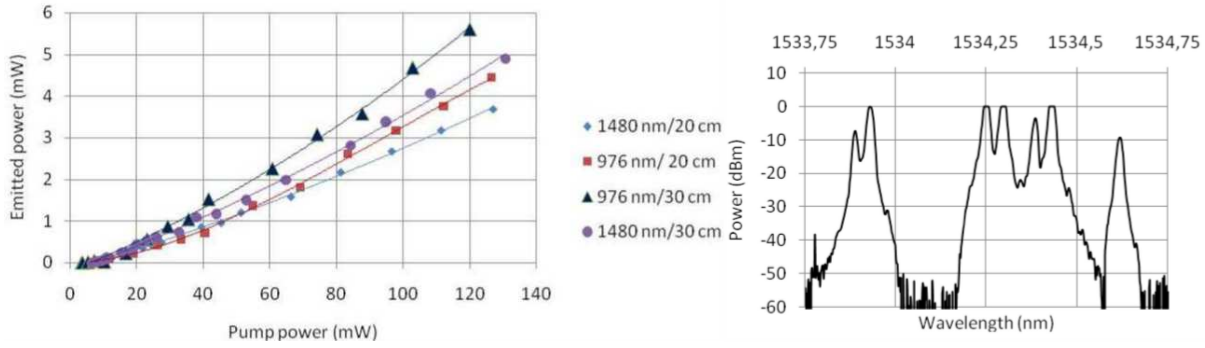

Figure 9 – **Er-Random fibre laser characterization, adapted from Reference (49)**. In left side, emitted power as a function of the injected power. Right side shown the emission spectrum of the 30 cm Er-RFL.

The right side of Figure 9 show the emission spectrum of the 30 cm device

pumped by a 1480 nm laser. At a pumping power far above the threshold, 120 mW, and the spontaneous emission is suppressed. It also shown the multimode behaviour of this laser. The 30 cm device is used in the works described in this thesis.

2 PHOTONIC SPIN GLASS IN ERBIUM RANDOM FIBRE LASER

This chapter presents the results of the statistics of the mode interaction in the intensity fluctuation in the spectral measurements of Random Laser.

The next section will describe the properties of the Erbium random fibre laser used in our work, as our measurements in the input output power characterization, the linewidth reduction and the estimation of the number of lasers modes with speckle contrast analysis. Following it, we review the thermodynamic spin glass and go to the analogy with photonics systems. From reviews of important results in this topic related with random laser, it introduces the reader into concepts used to analyse our results and ends with the statistical concepts presented in the text using our experimental results. Initially, we introduce to the spin glass transition, using some easy examples. If more details are need, the references in the text are pointed out. The results of this chapter were published in Reference (58).

2.1 Our results: Characterization of the Erbium random fibre laser

The same fibre (30 cm) employed in Reference (49) was used to develop the work that will be described. We performed the laser output emission versus the input power. In our results, the 30 cm Erbium doped random fibre laser was also pumped by a 1480 nm cw laser. We measured a laser threshold $4\times$ larger than the value reported by the authors in the Reference (49). It happens as a consequence of the fibre component used. As the injection of light is through fibre connectors, give rises to losses on the absolute power transmitted to the FBG. The fibre fusion splices used also introduces loss. After some time, we did the characterization using better quality splices and connectors, and we measured a laser threshold only $2\times$ large than the reported in the Reference (49).

2.1.1 Laser input output characterization of random fibre laser

As all the statistical analysis in this work depend on the power threshold, and not on absolute power value. We did all analysis normalizing the pump power by the pump power threshold, using the ratio P/P_{th}. The spectra below and above the laser

threshold are depicted in Figure 11 (a), four representative average spectra are shown. A 86142B Optical Spectrum Analyser (see Figure 10) with resolution set to 0.06 nm was used to measure the emission spectrum, and a sequence of 1500 spectra was collected for each pump power, with the sweep time set to 776 ms to acquire one complete spectrum.

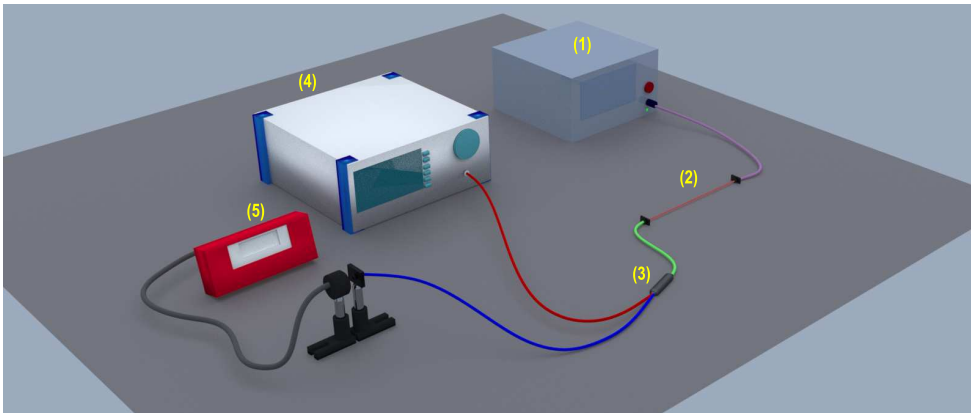

Figure 10 – **Experimental setup used to intensity fluctuation analysis**. A 86142B Optical Spectrum Analyser (4) with resolution set to 0.06 nm was used to measure the emission spectrum, the swept time measuring each spectrum was 776 ms. A 1480 nm pump (1) diode laser was used to pump the 30 cm Erbium-RFL (2), a wavelength divisor multiplexing (3) split the pump and signal, and the pump power is monitored by a power meter (4).

The spectra are averaged over 1500 measurements. The pump was a cw diode laser operating at 1480 nm. The RL emission was around 1543 nm. A sharp linewidth reduction is observed, reducing from $17,85$ nm to 0.06 nm, and its value is limited by the instruments' resolution of 0.06 nm, that is why we didn't observe spikes representative of the longitudinal modes as observed in (49). The emission spectrum for pump power below to above the laser threshold are showed in Figure 11 (a). While Figs. 11 (b) and 11 (c) shows the full width at half maximum (FWHM) (red diamond) and emitted intensity (blue circles) as a function of the pump power, which was varied in steps of $\approx$1.0 mW from 6 mW to 28 mW, in steps of $\approx$ 10 mW from 28 to 38 mW, in steps of $\approx$20 mW from 38 mW to 70 mW, and in steps of $\approx$30 mW from 70 mW to 90 mW. From the data of the emitted intensity, the threshold value of 16 mW was measured, which is very different from those of Reference (49). This is due to the high insertion loss of some of the components used in our experimental setup shown in Fig. 10.

This characterization was repeated before each experiment, for all the results

presented in this work. The goal was to all the times know the actual value of the random laser threshold P/P_{th} and the relatives input power P/P_{th}. The maximum output power emitted by the Er-RFL was ≈ 1.5 mW, pumped by 100 mW. The behaviour is always the same in relation to the threshold and it is a function of the threshold value, and do not depend on the absolute pump power value.

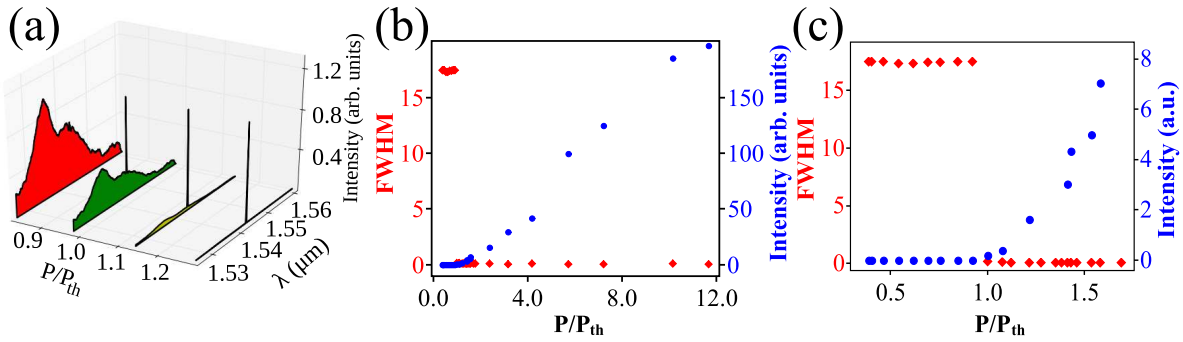

Figure 11 – **Random laser characterization results**. Spectral shape evolution (a), as a function of the pump power P normalized by the threshold power P_{th}. (b) FWHM (triangles) and emitted intensity (circles) as a function of P/P_{th}. The characterization near threshold pump power is in (c), showing the threshold inferred from the FWHM and output intensity versus input power.

A first thing that comes from a careful observation of these results and comparing with a spin glass system is: To observe the photonic analogue of spin glass system (that will be described below) a multimode laser emission is necessary to have mode interaction. It is not observed in the results showed in the Figure 11 (a). Spikes are averaged out during the measurement and cannot appear. To demonstrate that this RFL is multimode, speckle contrast measurement was employed to estimate the number of mode present in this system. The same illumination setup applied in the Reference (25) was used, as shown in Figure 12. A scattering medium with a dried TiO_2 nanoparticles of 250 nm average dimension was used to generate speckle. The transmitted light was captured by, a CCD (400 nm – 900 nm) and an infrared camera (0.4 μm – 1.9 μm).

For a mono-mode laser, as result of the spatial coherence, the scattering medium will introduce some bright spot in the image of the transmitted light. The addition of different laser mode will introduce another pattern of speckle contrast. The image acquired when the illumination is done by a multimode laser can be interpreted as a sum of m speckle patterns generated by each different mode. The sum of the average intensity value over all camera pixel $\langle I_q \rangle$ is $\langle I \rangle = \sum_q \langle I_q \rangle$, with variance $\sigma^2 = \langle I^2 \rangle - \langle I \rangle^2$.

When the measured speckle image is considered as a sum of m independent speckle patterns, of distinct laser modes, with probability distribution

$$P(I) = \frac{m^m I^{m-1}}{\Gamma(m)\langle I\rangle} \exp^{\frac{-mI}{\langle I\rangle}} \tag{2.1}$$

where I is the intensity sum over all the pixels, the number of laser modes is related to the speckle image contrast and can be estimated by

$$C = \frac{\sigma}{\langle I\rangle} = \frac{1}{\sqrt{m}} \tag{2.2}$$

where σ is the standard deviation, $\langle I\rangle$ the average speckle intensity, and m is the number of lasers modes.

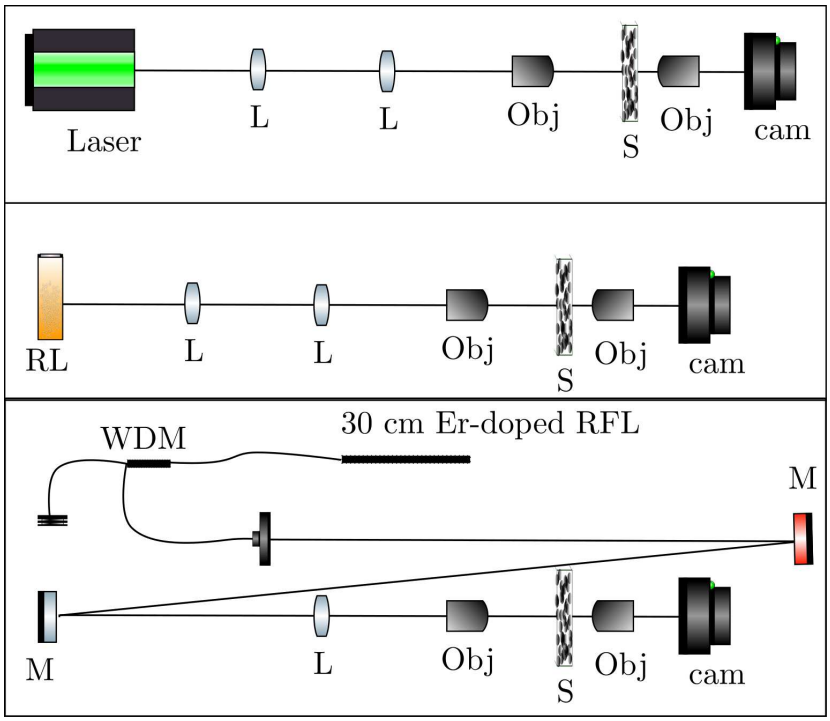

Figure 12 – **Experimental setup used to acquire the speckle images**. Three lasers was characterized, conventional laser (upper image), Rhodamine 6G dye RL (middle) and the RFL (bottom). For the RFL a wavelength divisor multiplex (WDM) and a dichroic mirror is used to remove the pump beam. And the symbols are L: Lens; Obj: objectives; S: scatter. Cam: camera.

The speckle contrast was measured from the central portion of the speckle pattern with an area of 600 $\times$ 600 pixels, to avoid optical aberrations produced at the edges of the sensor. This area was divided into sub areas of 80 $\times$ 80 pixels, obtaining the contrast for each subdivision and averaging these results. The system was tested with a 632.8 nm cw helium-neon laser, yielding a contrast of C = 0.81, equivalent to $\approx$2

modes. The speckle contrast of the Erbium RFL emission pumped by a 1480 nm cw laser, and operating far above the laser threshold, was measured as C =0.070, which correspond to m ≈204 modes. We also measured the contrast for this device pumped by a 980 nm cw laser, and the contrast value obtained of C =0.065, is quite similar to the 1480 nm pumping case, with m ≈236 modes. Such measurements of the number of modes are nearly equivalent as this value give us only a estimative.

For validation of the experimental setup, we measured a well-characterized RL based on a Rhodamine 6G dye and 250 nm TiO_2 particles, pumped by the second harmonic (532 nm) of a pulsed (7 ns, 5 Hz) Nd:YAG laser. A contrast of C =0.058 corresponding to m ≈297 modes was measured. The speckle contrast data are shown in Fig. 13, the speckle images (a), (c) and (e) are respectively the second harmonic (532 nm) of a pulsed Nd:YAG laser, 980 nm cw semiconductor laser and 1480 nm cw semiconductor laser. The RL speckle free regime, similar to the Reference (25) and using the same experimental setup as shown in Figure 12, can be observed in the Figure 13 (b). These results are also summarized in table 1.

Table 1 – Contrast ratio C and number of modes m for conventional lasers and random lasers. The Er-RFL system pumped by a 980 nm or 1480 nm diode laser displays $m = 236$ and $m = 204$ modes, respectively. A Rhodamine 6G dye random laser pumped by a second harmonic of a Nd:YAG laser shows $m = 297$ modes.

Laser	Contrast & number of modes
Second harmonic of an ND:YAG laser, @ 532 nm	$C = 0.71$, $m = 2$
Diode laser, @ 980 nm	$C = 0.54$, $m = 3$
Diode Laser, @ 1480 nm	$C = 0.70$, $m = 2$
Rh6G+TiO_2 RL, @ 590 nm	$C = 0.058$, $m = 297$
1D Er-RFL pumped by a 980 nm diode laser, @ 1540 nm	$C = 0.065$, $m = 236$
1D Er-RFL pumped by a 980 nm diode laser, @ 1540 nm	$C = 0.070$, $m = 204$

The results in this section showed the typical laser characteristic of the Er-RFL. The linewidth reduction and increase in the emitted intensity are observed for large gain. The spectral results, limited by instrumentation, show a single smooth spectrum. However, with the speckle measurements, we demonstrated that it was only because of the lack of a better experimental setup to make the measurements, and the behaviour is multimode. In the next section, the spin glass systems are introduced.

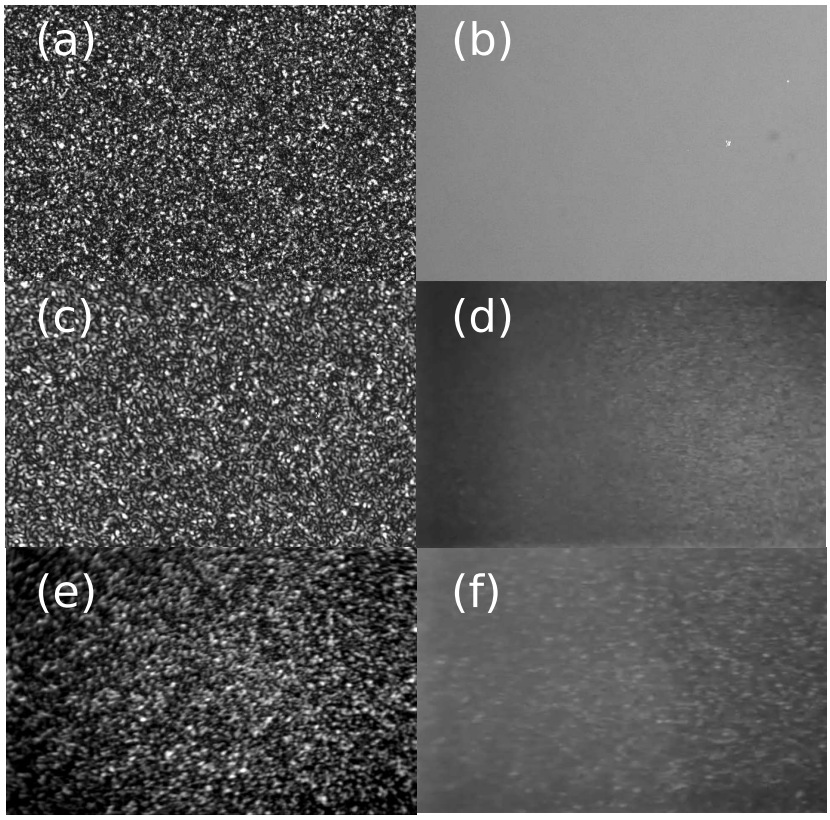

Figure 13 – **Speckle measurements images**. Speckle images of (a) a second harmonic (532 nm) pulsed Nd:YAG laser, (b) Rh6G-TiO2 RL (590 nm), (c) 980 nm semiconductor laser, (d) Er-RFL pumped by 980 nm laser, (e) 1480 nm semiconductor laser, and (f) Er-RFL pumped by 1480 nm laser.

2.2 Spin glass system

Spin glass is a system where its properties can be determined by disorder and frustration. In magnetic systems, the interaction of the spins magnetic moments at low temperature state are randomly disordered, and frozen. The two indispensable ingredients for spin glass state are lack of order and conflicting constraints (59, 60).

The disorder comes from the partially random interaction between the spins. It can be a mixture between ferromagnetic and anti-ferromagnetic interactions. The frustration occurs when a spin is in a state that it is not snuggled. It can be an effect from the competition introduced by the random interaction between the spin magnetic moments and, give rises to conflicting constraints in the lowest energy state. Using the Figure 14 it is easy to have a picture of these two concepts. Let's define black circles as spins oriented "up" and white circles as spins oriented "down". The interaction between the magnetic moments of the spins, ferromagnetic and anti-ferromagnetic interaction

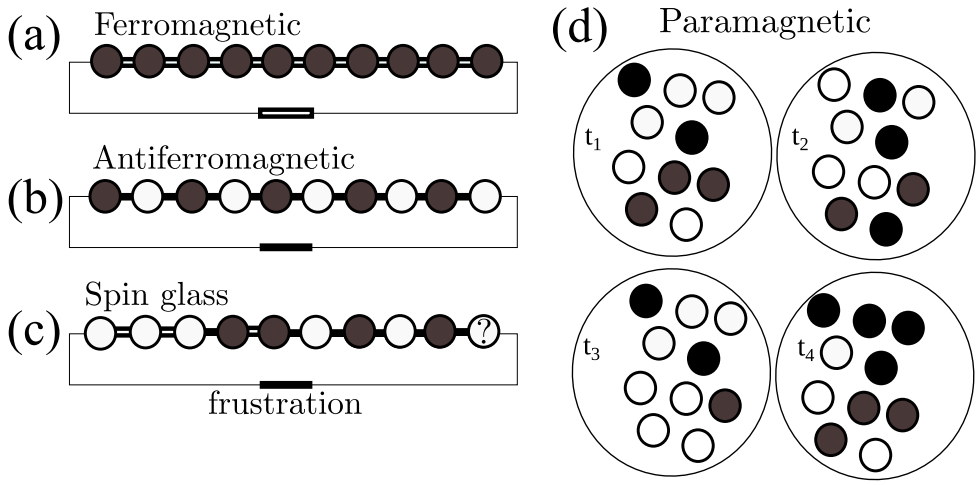

Figure 14 – **Scheme of spin interaction**. The circles are nodes and the colour represent the spin orientation. In the ferromagnetic case (a) are oriented in the same direction (same colour), antiferromagnetic interaction (b) neighbour spin oriented in different direction (different colour). The spin glass system (c) is represented as a system with frustration. In (d) each circle represent a different time t of observation on the spin orientation in a paramagnetic system.

are sketched as two lines connection and black line connection between the circles, respectively.

In a system formed by ferromagnetic interaction, Figure 14 (a), the spins must be parallel oriented, and the opposite happens in anti-ferromagnetic interaction system Figure 14 (b). In a spin glass system, the interaction is set as mixture between the last two cases in a random distributed pattern (disorder). The two magnetic interactions are present, and when the system temperature goes down carrying the system to the lowest energy state, spins start to be randomly oriented as a consequence of the interaction pattern, and then frozen-in. As a result, some conflicting spin orientation arises. Figure 14 (c) illustrate this scenario. In any position that the last spin (labelled with "?") stay, it will be in an discomforted situation. In the Figure 14 (c) it is represented as two consecutive anti-ferromagnetic interactions. The right edge spin orientation is undetermined as its left neighbour is black the spin needs to be white meanwhile the spin is also forced to be black as its right neighbour is white. This indeterminacy is an example of what is called frustration. In the spin glass systems, the disorder must produce frustration to be relevant. Figure 14 (d) shows an example of paramagnetic interaction, the spin orientation at high temperature is non-longer determined by the

individual interaction between the spin, as it can couple to external sources, each circle in Figure 14 (d) represents the spins' configuration at different time.

The macroscopic magnetic properties of this system, the magnetization, in average is

$$\mathbf{M} = (1/N)\sum_i \langle \mathbf{M}_i \rangle = 0$$

.

The order parameter $\mathbf{M}$ is zero at high temperature, and goes to ± 1 as the temperature decrease to a point below of a critical temperature T_c. The main difference from a spin glass system, is that the spin are not frozen in the paramagnetic state case.

The name spin glass is due the analogies with chemical glass, as it is composed by atoms that had stuck in random position in a structural disordered way (61). Instead of structural disorder, the thermodynamic spin glass system is composed by interaction disorder.

2.2.1 A simple model

The Ising spins are an example of thermodynamic glass system (59)[1] The model is a periodic lattice of N molecules (nodes), to each node a spin variable with values $S_i = \pm 1$ is set, each spin can be only up or down. The exchange energy between first neighbour nodes i and j is given by J_{ij}. When $\mathrm{J}_{ij} > 0$, neighbouring spins have the same S value. And conversely have different S values if $\mathrm{J}_{ij} < 0$. The internal energy, for a zero external magnetic field, is given by:

$$H = -\sum_{\substack{i,j \\ i \neq j}}^{N} \mathrm{J}_{ij} S_i S_j \tag{2.3}$$

where N is the number of nodes, $S_{i,j}$ takes values ± 1 ($i, j = 1, 2, ..., N$), i and j are the spin labels. J_{ij} is a quenched random spin to spin interaction with a Gaussian distribution function. In this case we consider non-zero interaction for nearest neighbours only. For a positive (negative) interaction, the product between two spins in the lowest energy state is positive (negative).

[1] Actually, this is called as *Edwards-Anderson Ising model*, and a more useful is the infinity-range Sherrington-Kirkpatrick Hamiltonian, as it does not include geometrical constrains . To a better (and straightforward) explanation of how this goes from the EA to SK model the chapters 3, 4 and 5 of the reference (61) and their references is a good start point.

Thus, consider a lattice formed by 9 nodes, as in Figure 15. The part (a) shows an example of a chain with positive interaction (two lines), spins aligned in the same direction (same colour). Figure 15 (b) shows negative (one line) and positive interactions (two lines) and the spins are aligned in both directions. In these cases (a) and (b) all spins are in a ground state determined by the interaction exchange energy, there is nothing to force breaking this rule, then the ground state of the system is easily determined. However, in the case of Figure 14 (c) there is also a mixture between positive and negative interactions, but contrary to the case of Figure 15 (a) and (b), this mixture of exchange energy creates frustration. Look to the centre node, and the fact that interactions are fixed, its easily to see that the spin is in an uncomfortable position. Any choice of the spin with the label "$?$" inside the circle result in a mismatch with the spins interactions and their orientation. So, in this case, the ground state of the system is degenerate.

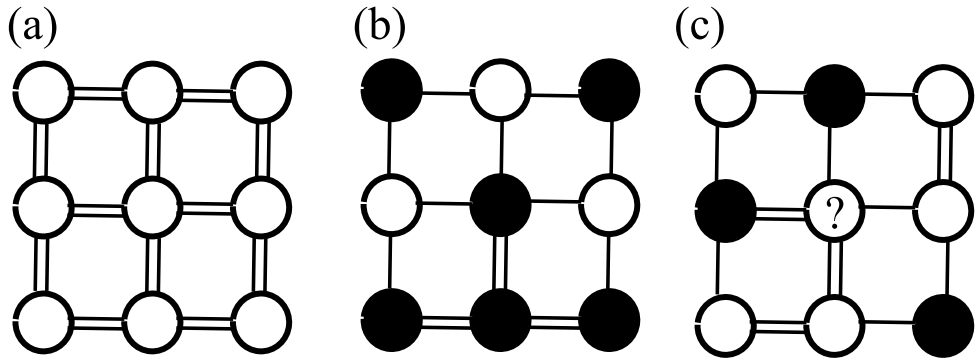

Figure 15 – **Example of a square lattice with disorder interaction**. (a) only positive interaction, (b) mixture with positive interaction without negative chain product and (c) with negative chain product.

As many nodes the frustrated system have, more degenerate can be the ground state. This means there is an energy landscape at the ground state, with valleys, that can trap the system. Then, if an EA Ising system formed by N nodes, at a temperature $T > T_c$, with fixed random interaction J_{ij}, the system is then in a paramagnetic state, where the average macroscopic magnetization $\mathbf{M}$ is zero, as the spins magnetic moment orientation are fluctuating in time. When the system is left to rest, it goes to the ground states and reach a determined spin configuration. In the case of a ferromagnetic system this only goes to a state with magnetic moments ± 1. Spin glass system behaves different, at each time the experiment is repeated, with the same initial condi-

tions, because of the degeneracy and the frustration introduced by disorder interaction, it is possible that the system goes to different valleys of the ground state energy landscape, with different spin configuration. The measured spin magnetic moment $\langle \mathbf{m}_i \rangle$ in each site i, can result a different value at each experiment γ.

Moreover, in each experiment the magnetic moment fluctuates from spin to spin. The degree of freezing of the system is given by the order parameter

$$q = \frac{1}{N} \sum_i |\langle S_i \rangle_\gamma|^2 \tag{2.4}$$

and give us information of the spin orientation inside a valley of the energy landscape. A order parameter $q_{\gamma\beta}$ is used to quantify the amount of proximity between the results in each experiment γ and β (59), and give us details about the possible valleys that form the energy landscape:

$$q_{\gamma\beta} = \frac{1}{N} \sum_i^N \langle S_i \rangle_\gamma \langle S_i \rangle_\beta \tag{2.5}$$

for $\mathrm{q}_{\gamma\beta} = 0$, there is no correlation between the measurement γ and β. As $\mathrm{q}_{\gamma\beta}$ increases more correlated are the states in the experiments γ and β. As we are interested in the whole system behaviour, a probability distribution to find the system in a specific state is statically described by

$$P(q) = \sum_{\gamma\beta} \delta(\mathrm{q}_{\gamma\beta} - q) \tag{2.6}$$

In the paramagnetic state, as the system is completely uncorrelated, the possible results for the Equation 2.6 is a peak centred at values zero of the order parameter. For ferromagnetic state, there are only two possible results for each node magnetization, and the function $P(q)$ has only two δ-functions at the values $\pm m^2$. In the spin glass state there is a continuous fragmentation of the valleys of states into smaller ones. The system can then freeze in different states, and then in the distribution function $P(q)$ a continuous curve between the δ-function appears. The maximum value of the $P(q)$ is called as selfoverlap, that means the most possible state to find the system (59, 61). The example aforementioned are sketched in the Figure 16. A more complete and detailed introductory treatment of spin glass can be obtained by the references (59, 61, 62, 63).

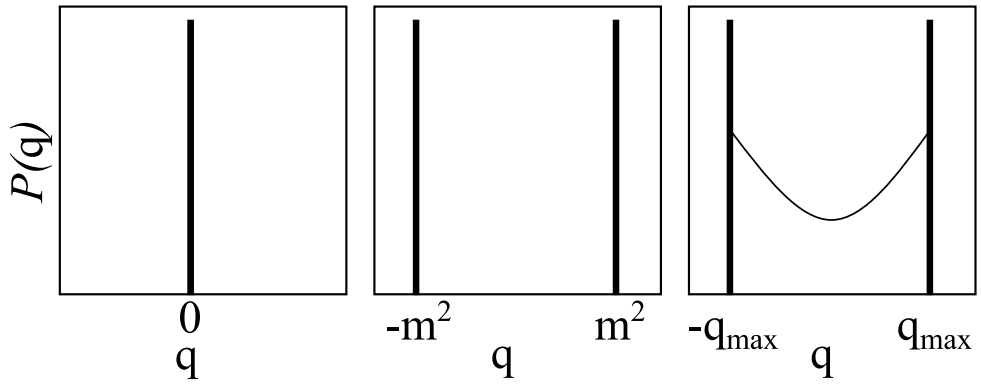

Figure 16 – **Examples of PDF order parameter** $P(q)$. The PDF $P(q)$ can show only a delta peak at $q = 0$ in the paramagnetic state, and $\pm m^2$ in ferromagnetic state. The glass state is described by the appearance of a continuous curve between the delta functions.

2.3 Random laser as photonic analogue to thermodynamic spin glass

Random lasers spectral emission has interesting properties, such that they can be used as physical statistical platforms, allowing the study of statistical phenomena in controlled systems. Using the intensity fluctuation spectra in random lasers, Ghofraniha (37) and co-authors demonstrated the first observation of the glassy behaviour of light in RL and replica symmetry breaking (RSB), i.e., an RL system under identical experimental conditions can reach different states characterized by different emission spectra. RSB theory predicts that, identical system, prepared under identical initial conditions, can demonstrate different results. It was observed that, the shape of the distribution function of an order parameter q, named as Parisi overlap, change their form from a peak centred at 0 to maxima with values $q \neq 0$. The RL were called as the photonics analogue of thermodynamic spin-glass systems.

This open cavity RL system pumped after certain power threshold (P_{th}) shows emission determined by long-lived modes with frequency k and spatial pattern $\mathbf{E}_k(\mathbf{r})$. It was experimentally observed that large fluctuation in the intensity emission occur when pump power is near the P_{th}, and still remain far after threshold, with less fluctuation intensity.

This behaviour was called shot-to-shot intensity fluctuation in RL, and not only the intensity, the actives' emission modes also can change in time, creating a shot-to-shot non-trivial spectrum fluctuation.

This shot-to-shot fluctuation resembles previously mentioned spin glass system, in the sense that the measured state where the system goes is the emitted spectrum. The Ising degree of freedom $S = \pm 1$ is related with the slow modes amplitudes contribution $a_k(t)$ to the electric field expansion

$$\mathbf{E}(\mathbf{r}, t) = \sum_k a_k(t)\mathbf{E}(\mathbf{r})e^{i\omega_k t} + c.c. \tag{2.7}$$

inside the material, with the oscillation period $1/\omega_k$ smaller than the relevant time scale for $a_k(t)$. The randomness in the material refractive index introduces the time independent disorder by the irregularity of the spatial mode profile in $a_k(t)$ modes interaction. As many modes are pumped and active, these are trying to oscillate coherently at the same time what gives rise to the photonic frustration. The system can be described by the Hamiltonian (40, 38, 64)

$$H = \sum_{\{jk\}'}^{n} \mathrm{J}_{jk} a_j a_k^* + \frac{1}{2} \sum_{\{j,k,l,m\}'}^{n} \mathrm{J}_{jklm} a_j a_k^* a_l a_m^* \tag{2.8}$$

where $\{\cdots\}'$ implies the frequency-matching conditions $|\omega_j - \omega_k| \lesssim \gamma$ and $|\omega_j - \omega_k + \omega_l - \omega_m| \lesssim \gamma$, with γ being the finite linewidth of the modes, J is the random interaction between the spins with PDF $P(\mathrm{J})$, j, k, l, m represent the laser mode label. By analysing the Hamiltonian of Equation 2.8 using the replica method (60), that is: As the interaction variable is unknown, but are random variables with a known probability distribution and quenched as J does not depend on the experiment time scale, it is necessary to analysis different realizations of the system, and computing it averages free energy. Thus, under the same set of random interaction variables, for N copies of the system the averaged free energy is evaluated (60, 38, 64)

$$F = -T\overline{\log Z_{\mathrm{J}}} = \lim_{N\to 0} \frac{\overline{Z_{\mathrm{J}}^N}}{N} \tag{2.9}$$

where the bar denotes the average over the J's configurations, the random laser pumping rate is $P \propto \sqrt{\frac{1}{T}}$,

$$\overline{Z_{\mathrm{J}}} = \overline{\sum_{\mathrm{J}} P(\mathrm{J}) Z_{\mathrm{J}}^N} \tag{2.10}$$

is the disorder averaged partition function of the N times replicated system. As the number of interaction into the system is sufficiently large, a self-averaged free energy is obtained (64). The order parameter between two system replicas a and b is given by

(38, 64)

$$Q_{ab} = \frac{1}{E}\sum_{k=1}^{n} a_k^a (a_k^b)^* \tag{2.11}$$

The glass phase in the random laser emission was proposed in (65), as a result of the large mode competition for the available gain in a quenched disordered system. In such case the modes do not oscillate with the same phase. The experimental access for measurement of the replica symmetry in random lasers is not easy. The emitted intensity $I_\gamma(k) = |a_k^\gamma|^2$ by the replica γ at the wavelength indexed by k is more experimentally accessible, and present a non-trivial fluctuation (8, 18), also the connection between the replica analysis of the mode amplitude and the intensity fluctuation was made in (38).

The experimental observation of the PDF in the replica analysis was made by Ghofraniha (37). The proposed order parameter to the intensity fluctuation overlap was

$$q_{\gamma\beta} = \frac{\sum_k \Delta_\gamma(k)\Delta_\beta(k)}{\sqrt{\sum_k \Delta_\gamma^2(k)}\sqrt{\sum_k \Delta_\beta^2(k)}} \tag{2.12}$$

where γ, $\beta = 1, 2, ..., N_S$, for each pump power, denote the replica labels, the average intensity at the wavelength indexed by k is $\overline{I}(k) = \sum_{\gamma=1}^{N_S} I_\gamma(k)/N_S$, and the intensity fluctuation is given by $\Delta_\gamma(k) = I_\gamma(k) - \overline{I}(k)$.

The experimental parameter $q_{\gamma\beta}$ can assume values in the interval $[0.1]$. Glass behaviour can be identified by the analysis of the point q that $P(q = q_{\gamma\beta})$ have its maximum. When the peak is centred at $q = 0$, no correlation is observed between the emitted intensities, the system is in a photonic paramagnetic phase. For $q \neq 0$, the intensities fluctuations are correlated $q = 1$ fluctuating in the same sign and same value in relation to the average, or anti-correlated $q = -1$ fluctuating in the same intensities but differs in the sign.

In Ghofraniha's paper was observed that the experimental PDF of the order parameter $P(q)$ changes from a distribution with peak centred at $q = 0$ below the pump threshold (high temperature), to a PDF $P(q)$ that present peaks at $q \neq 0$, with a continuous curve between those peaks, as the system pump power (temperature) increases (decreases). This observation signalizes to the glass phase of light, where the intensity fluctuation, in relation to the average emitted spectrum, at each wavelength k, are correlated as a result of the mode competition by the gain. Such behaviour was

also observed in bulk colloidal dye-nanoparticles RL (45) and rare earth doped powder RLs (40).

2.4 Our Results: Glass behaviour on the Erbium-RFL

So far, there is no demonstration of the spin glass system in one dimensional random laser. A fibre optics is employed to obtain an approximation of a one-dimensional laser. Here we describe a spin glass behaviour on the 30 cm Erbium random fibre laser (Er-RFL).

2.4.1 Characterization of RSB Phase transition

The order parameter $q_{\gamma\beta}$, is used to quantify the RSB phase transition from photonic paramagnetic to the spin-glass RL behaviour. This order parameter is similar to the Parisi overlap parameter in spin-glass theory (61, 59). This parameter can be calculated either among the mode's amplitude a_j or intensities $I_j \propto |a_j|^2$, the latter is more accessible experimentally and both are similar. By measuring fluctuations in the intensity averaged over N_S system replicas, the overlap parameter is (37)

$$q_{\gamma\beta} = \frac{\sum_k \Delta_\gamma(k)\Delta_\beta(k)}{\sqrt{\sum_k \Delta_\gamma^2(k)}\sqrt{\sum_k \Delta_\beta^2(k)}} \tag{2.13}$$

where γ, $\beta = 1, 2, ..., N_S$, with $N_S = 1500$ for each pump power, denote the replica labels, the average intensity at the wavelength indexed by k reads $\overline{I}(k) = \sum_{\gamma=1}^{N_S} I_\gamma(k)/N_S$, and the intensity fluctuation is given by $\Delta_\gamma(k) = I_\gamma(k) - \overline{I}(k)$, k is the wavelength of each point of the spectrum, in the experimental data it is labelled from $0, 1, \cdots, N_k$.

In this experimental procedure using a 1480 nm cw pump laser, each emission spectrum collected with the time frame of 776 ms is considered a replica of the system. i.e., a copy of the RL system under identical experimental conditions, and random scattering medium fixed. The spectra collected, or each replica of the system, below, near and far above the laser threshold are in the Figure 17, (a), (b) and (c) respectively. The replicas are labelled from 0 to 1499, and the wavelength measurement window is from 1528 nm to 1560 nm. The Equation 2.13 give the information of how the fluctuation at each wavelength indexed by k in relation to the average is correlated to each other. That is, there is a value for the parameter $q_{\alpha\beta}$ that describes the correlation of each fluctuation of one spectrum α to another spectrum β. With it a histogram of all $q_{\alpha\beta}$ is

realized (experimental $P(q)$), and the point of maximum occurrence determines the point where the system can more probably founded.

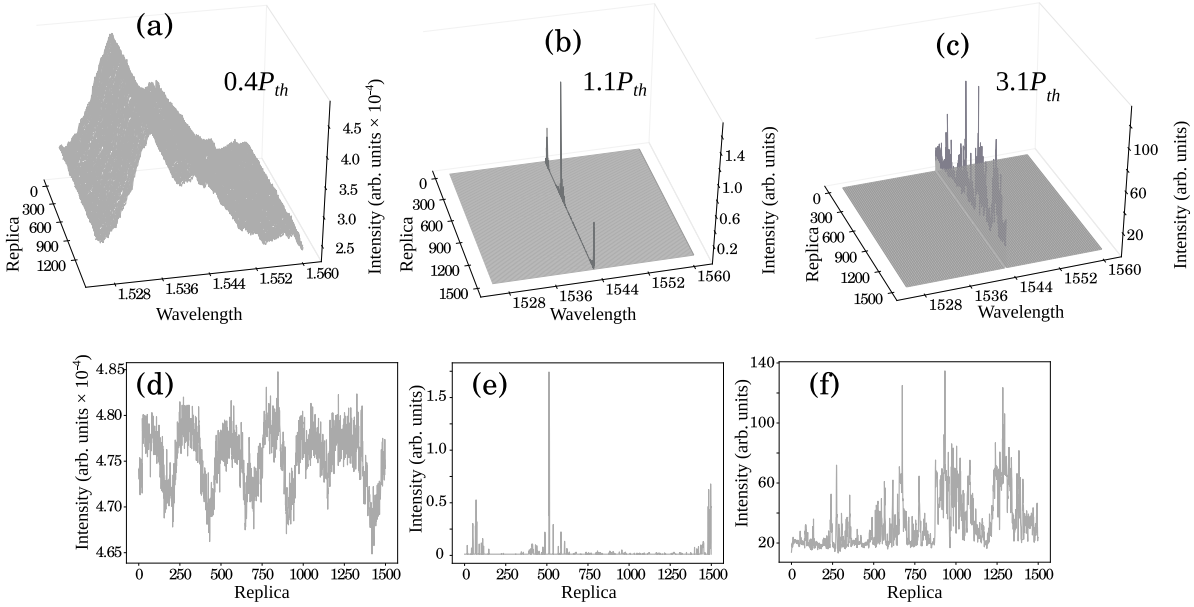

Figure 17 – **Random laser emitted spectra**. Representative emission spectra from below (a) near (b), and above the random laser threshold, and the respective intensity fluctuation as a function of the pump power (d-f).

The probability density function (PDF) $P(q)$, analogue to the Parisi order parameter in RSB spin-glass theory (37), describes the distribution of the replica overlap $q = q_{\gamma\beta}$, signalling a photonic uncorrelated paramagnetic or a RSB spin-glass phase, if peaks are exclusively at q =0 (no RSB) or also at values $|q|$ ≠0 (RSB).

Figure 18 shows the $P(q)$ evolution as a function of the pump power from below (a-b), through around (c-d) to above (e-i) the random laser threshold, characterizing the phase transition from photonic paramagnetic phase ($q_{max} = 0$) to spin glass phase transition $q_{max} \neq 0$. Figure 19 shows the value $|q| = q_{max}$ at which the $P(q)$ assumes the maximum. For $|q_{max}| = 0$ the system is most probable overlap to a non-correlated state, i.e., all the modes oscillate independently and do not interact. For $q_{max} = 1$ the modes interact and are no more independent, their fluctuation are correlated, $q_{max} = 1$ (fluctuate in the same direction and similar amplitude in relation to the average) or $q_{max} = -1$ (fluctuate with similar amplitude in different direction).

A sharp transition coinciding with the threshold is observed from the photonic paramagnetic (Figs. 19, below P_{th}) to the spin-glass phase (above P_{th}). Figure 19 (a) displays q_{max} for pump power below and above P_{th} (up to 2$_{Pth}$), together with the emis-

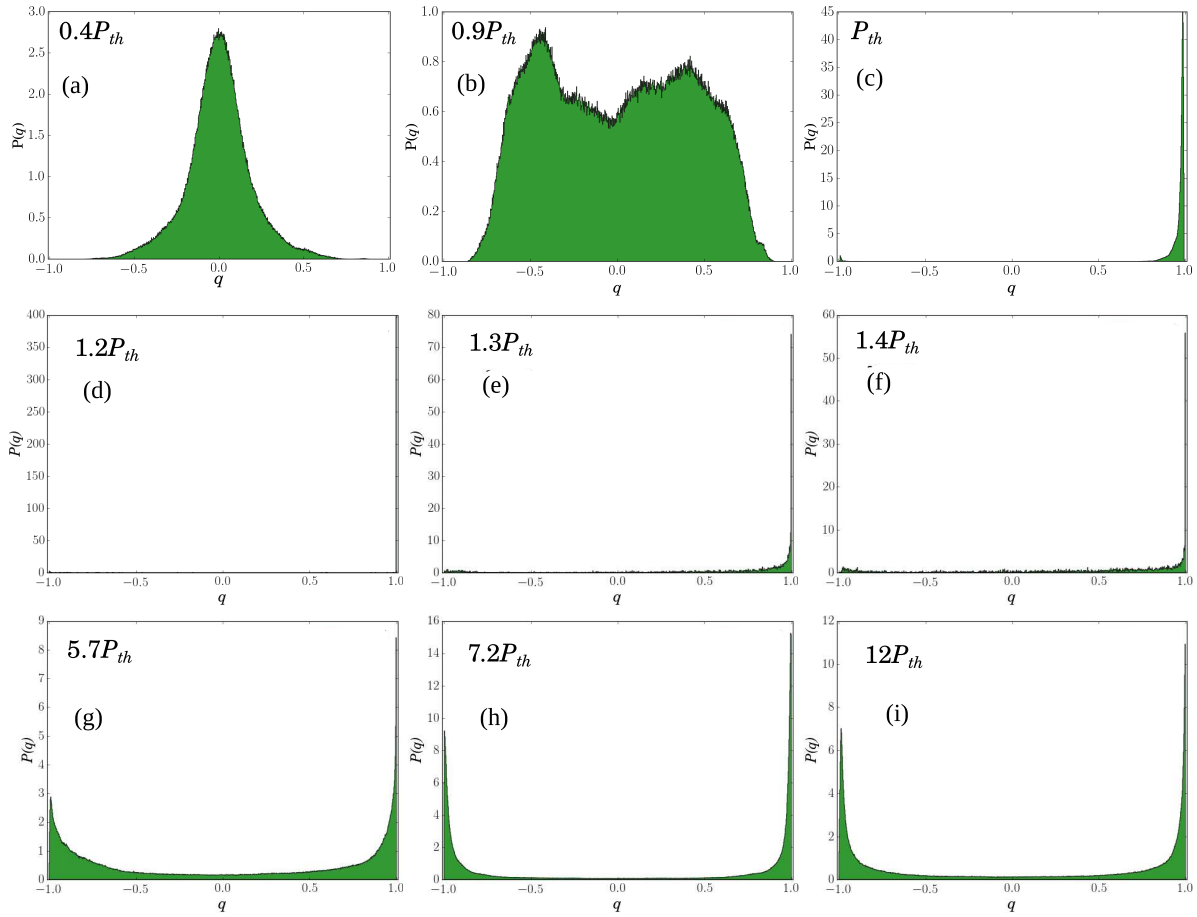

Figure 18 – **Observation of RL glass behaviour in RL**. PDF $P(q)$ obtained from experimental data at the indicated pump power (normalized with respect to P_{th}), showing the random laser phase transition from the photonic paramagnetic regime (a,b) to the spin glass transition (c-i).

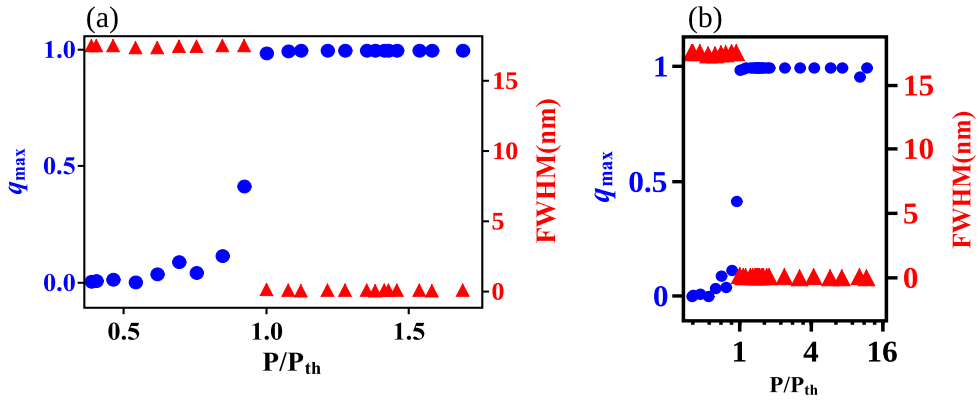

Figure 19 – **Replica symmetric breaking as RL threshold determination**. Value $|q| = q_{max}$ at which $P(q)$ assumes the maximum (circles) as a function of the normalized input power together with the FWHM (triangles) for the sake of comparison with the random laser threshold.

sion linewidth reduction for the sake of comparison. The results for pump power up to $12P_{th}$, showing the steady behaviour, are in Figure 19 (b).

2.4.2 Summary

As a summary, we used a RL system where the disorder scattering medium is formed by a continuous FBG with random phase errors, instead of the presence of random scattering particles (22), such medium is static and scatterers do not influence the pump beam. The multimode characteristic of the Er-doped random fibre laser was confirmed, as it is necessary to a RSB phase transition that relays on the mode interaction regime.

Regarding the RL space dimensionality, we showed, for the first time, that the replica symmetric theoretical approach also works in 1D random laser. Actually, by taking the random couplings as Gaussian variables in the photonic Hamiltonian, the explicit connection with the spatial structure of the disordered nonlinear medium is lost. This reasoning is reinforced by the fact that, while the summations in the magnetic spin Hamiltonian run over the spins positions in the lattice (which take into account the geometrical structure), the sums in the photonic Hamiltonian are over the mode labels, which keep no structural link with the background medium, not depending on the system geometry. In conclusion, we have demonstrated a photonic spin glass phase in an Er-doped RFL. This can be observed in the $P(q)$ evolution, confirming the role of the RL modes as analogues to disordered spins from the thermodynamic spin glasses. The multi-mode behaviour was confirmed by speckle contrast measurements. And the results also show that this transition undoubtedly coincides with the RL threshold, confirming previous results (37, 40) on different dimensions. The evidence of RSB in the cw regime also opens up important possibilities for new experimental demonstrations of other expected transitions.

3 INTENSITY FLUCTUATIONS IN RANDOM LASER

RL output emission can present high intensity fluctuation. Around a determined pump power injected into the RLs, the system can reach the threshold and comes back to below threshold (24, 66), in a laser-no-laser behaviour. This can be related to the high sensitivity to the initial conditions and mode competition due the extended modes' character. A Lévy like distribution in this regime is observed (67), and the degree that the system goes inside of this non-Gaussian regime can depend on the scattering strength and external parameter (68). In this chapter we will present the Lévy-like behaviour of the random fibre laser emitted intensity.

3.1 Lévy distribution

The Lévy distribution presents a divergent variance because of the high intensity fluctuation and is also called by fat tail distribution, with non-zero probability for events localized far from the average value. The probability distribution follows a power law, that violates the central limit theorem in the presence of an infinity variance. In physical systems, a probability density function with a diverging second moment represents an unphysical possibility. In any system of stochastic variables statistically independent and identically distributed, with finite second moments, a Gaussian distribution is obtained (69). The addition of a boundary limit to the probability distribution, e.g., $P(X) = 0$ for $X > X_{max}$ or by tempering the power law with an exponential attenuation ($P(X) \sim X^{-\mu} \exp(\eta I)$) (69, 29), with large finite moments has a Lévy like behaviour with an ultra-slow convergence to a Gaussian regime. Actually, the aforementioned is *Lévy like* intensity fluctuation of random laser as it has a large but finite variance, with a truncated Lévy distribution with finite moment.

The Lévy distribution can be found in systems like financial market and food search by albatrosses (70, 71, 72). The distribution can have the form of $P(I) \sim X^{-u}$ with number of samples of the set $\{I\} \to \infty$, for (73),

- $u \geq 3$ the variance is finite, and the central limit theorem is applied and a Gaussian distribution is recovered.

- $u < 3$ the variance starts to diverge and a broad distribution appear, and the central limit theorem is not more applied and states that a non-Gaussian distribution govern the system.

3.1.1 Lévy walks

Like as Gaussian distributions, Lévy is also a stable distribution, a random walk that have heavy tail distribution can be viewed as a sequence of localized Gaussian random walk connected by large jumps with no points between the start and end point of the jump, also known as Lévy flights. This is sketched in Figure 20 (b), while in (a) Gaussian random walks is shown for completeness and comparison. The first 1000 step random walk is simulated, starting from the position $(x, y) = (0, 0)$, the step can go to any angular direction with uniform distribution. The step size is generated with a Gaussian distribution $\alpha = 2.0$, centred at 1.0 (Figure 20 (a)). The Lévy step size distribution is simulated with $\alpha = 1.6$ and location parameter also 1.0, showing step size of tens and hundreds of units.

Stable distribution with the Fourier transforms to the k-space, can be described by the family of α-stable distribution given in the k-space by the equation:

$$\overline{P}(k) = \exp\{ikv - |ck|^{\alpha}[1 - i\beta \mathrm{sgn}(k)\Phi]\} \tag{3.1}$$

In Equation 3.1 the Lévy index $\alpha \in (0, 2]$ is the most important parameter, since it holds the type of statistics that characterizes the system of random variables. Strong fluctuations in the random variable with relevant deviations from the Gaussian behaviour are associated with values in the range $0 < \alpha < 2$, and the boundary value $\alpha = 2$ recovery the Gaussian distribution. The parameter $\beta \in [-1, 1]$ carry information of the asymmetry of the distribution, v drives the location and c is a scale parameter. The other $\Phi = \tan(\pi\alpha/2)$ if $\alpha \neq 1$, whereas $\Phi = -(2/k)\ln|k|$ if $\alpha = 1$. The Lévy PDF displays closed analytical form only for a few values of α.

Examples of α-stable PDF are in Figure 21. The PDF was numerically obtained with the algorithm provides for python (74). The α parameter assumes values that varies from 0.8 to 2.0 in steps of 0.4. And the skewness parameter is $\beta = 1.0$ Figure 21 (a), $\beta = 0.0$ Figure 21 (b) and $\beta = -1.0$ Figure 21 (c). The fast decay of Gaussian distribution when compared to a Lévy is depicted in the insert of Figure 21 (b). As large is the α faster will decay the PDF for large X values. For skewness $\beta > 0$ (a) the

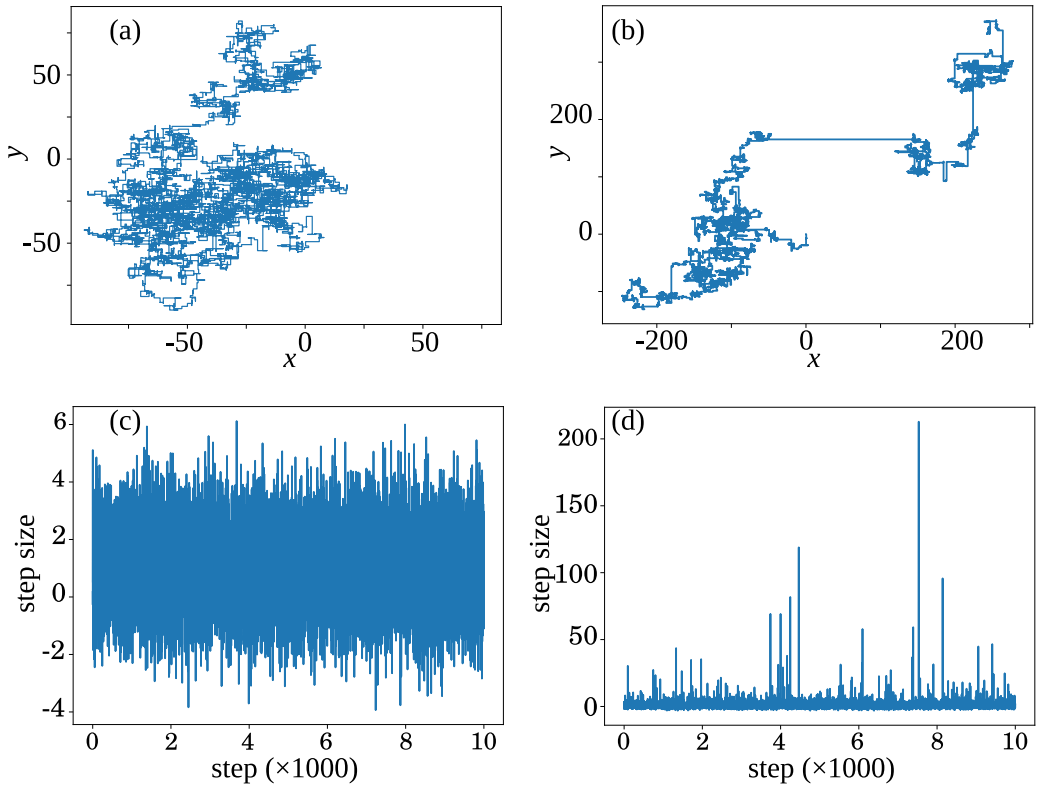

Figure 20 – **Example of random walk with the path length determined by the alpha stable distribution**. Path length determined by the α-stable when $\alpha = 2$ (a), and $\alpha = 1.6$ (b), In both cases the location parameter is 1.0 and the skewness parameter is 1.0. Observe that for the Lévy-like case, the path shows long lines connecting small paths. Also, the step size as function of the step label number is in (c-d).

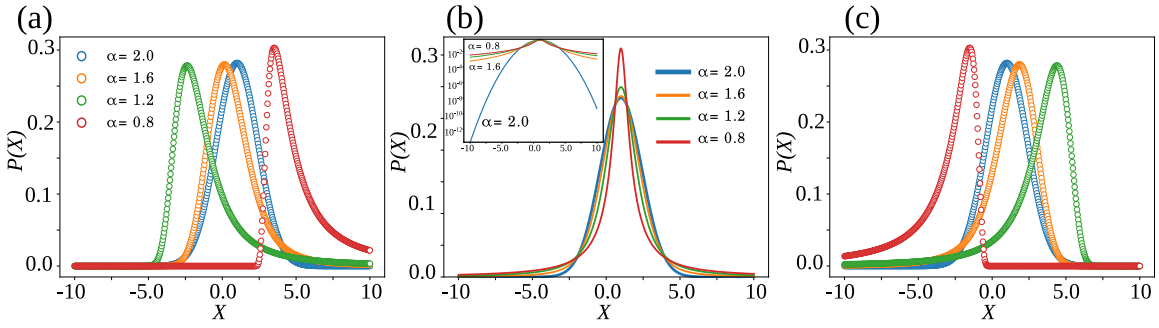

Figure 21 – **Alpha stable function examples**. In all the cases the α parameter assumes the values 2, 1.6, 1.2 and 0.8, and the β values are 1.0 (a), 0 (b) and -1.0 (c). The insert of (b) shows the asymptotic decay difference between the Gaussian to Lévy regime in log scale. The Gaussian distribution faster goes to zero as x increases.

large vales of intensity fluctuation are for positive x, and for negative x (c) when the skewness is negative.

3.2 Lévy intensity distribution in random laser

The laser threshold determination in conventional laser is usually inferred by the point where the emission intensity diverges (1), the system has a well-defined point where its emitted intensity, at a certain wavelength determined by the cavity geometry, goes to laser operation regime. It is not often observed in RLs, where the open cavity character makes that a preferred laser emission is not present (12), and after a certain pump energy, the system can start a *laser-no-laser* behaviour jumping from below to above and backs to below threshold (66) making difficult to determine the exact pump energy threshold. Rare long-lived extended modes that can occupy a region larger than the amplification length, can dominate over the others, retain most of the gain resulting in a large amplification. They can generate large intensity fluctuation as a result of the variation of the length of these modes. This behaviour of large intensity fluctuation was observed in several experiments (12, 66, 67).

3.2.1 Observation of Lévy distributions in the intensity emission of bulk RL.

The presence of Lévy statistic in random laser intensity fluctuation was demonstrated in Rhodamine 6G based random laser (67). The formation of a fat-tailed probability distribution of the emitted intensity was observed. A Lévy behaviour increases with scattering concentration, and the author argues that a non-uniform gain distribution was the origin of it. The characteristic α parameter was also proposed as proportional to the transport and gain length, which variation shows the transition from the Gaussian to Lévy-like behaviour.

S. Lepri *et al.* in Reference (75) studied the different statistical regime present in random laser. Using a diffusive model, they derive the emission probability which depends on the gain and scattering mean free path length:

$$p(I) = \frac{l_G}{\langle l \rangle} I^{-(1+\alpha_d)},\ \alpha_d = \frac{l_G}{\langle l \rangle}. \tag{3.2}$$

The Lévy exponent for it diffusive regime α_d determines if the power law follows a Gaussian $\alpha_d > 2$ or a Lévy distribution $\alpha_d \leq 2$. The author suggested that the random intensity fluctuation has a transition from Gaussian to Lévy and vice-versa depending on the sampler parameter as gain length and scattering concentration. Also, they well predicted that the Lévy intensity fluctuation Regime occur around the RL threshold.

G. Zhu et. al (44) demonstrated that the random laser threshold can have a Lévy-like intensity fluctuation. They also showed that the Lévy intensity fluctuation in their ceramic-based RL is not related to the fluctuation of the pump source. Indeed, even with high stable pump the fluctuation is large around the threshold.

The works aforementioned fail to make a detailed studied of the intensity fluctuation dependency on the pump energy, moreover the analysis used in their works was not easily adapted from one to another system.

R. Uppu and S. Mujumdar proposed a method to identify the statistical regime of the intensity fluctuation, in the output emission of RLs, using the α-stable distribution (28), Equation 3.1. The sample of study was a canonical Rhodamine 6G based random laser, ZnO nanoparticles of 20 nm diameter as scatterers, pumped by the second harmonic of a Nd:YAG laser of 30 ps pulse duration. With the analysis of 2000 spectra, the authors estimate the parameter of the α-stable distribution. The tail exponent α shown three different behaviour. The first was when the probability of random laser emission is zero, and the alpha stable distribution parameter of the fluorescence emission is $\alpha \approx 2$.

The regime where the probability of random laser P_{RL} grows in the interval $0 < P_{RL} < 1$ the tail parameter decreases from $\alpha = 2$ to $\alpha \approx 1$, where more modes are activated, and the intensity fluctuation become large, and then increases again to $\alpha = 2$, with the minimum values where the probability of random laser P_{RL} approximate to 0.5. The third was for laser behaviour far above the threshold, where a new Gaussian regime is recovered, and $P_{RL} \approx 1$. This method also agrees with the linewidth reduction and intensity increases of the emitted spectra.

The intensity fluctuation regime in RL is dependent on the scattering strength. When the mean free path increases the intensity fluctuation also increases, thus the system goes deeper into the Lévy regime and more slowly goes back to the Gaussian (68). In the sense of photons path, high intensity emission is explained: as large is the path travelled by the photons then higher is the amplification, and such photons retain almost all gain. The fluctuation in the path length from each path realization reflects in the intensity fluctuation.

3.2.2 Lévy statistics in the random laser transition

A detailed study of the Lévy distribution in the random laser threshold was made by Ignesti *et. al* (68). They realized a numerical simulation and also experimental study, the results shown a statistical transition that follows the random laser transition from the regime pre-lasing to laser regime, e.g., α-stable parameter curve as a function of the pump energy shows a negative slope change, the stable distribution characterized by an $\alpha = 2$ goes to $\alpha = \alpha_{min}$ near the pump power threshold. As the system goes near the laser regime the slope again change, but now for a positive value and thus goes back from the $\alpha = \alpha_{min}$ to the maximum value $\alpha = 2$. Such behaviour is sketched in Figure 22, the continuous curve represents the form of the alpha stable curve as a function of the pump energy, and it is compared to the FWHM reduction (a) and intensity increases (b) after the threshold. The α parameter reaches the minimum value when is near the threshold, where the modes' activation starts. The curve remains constant in the pre laser regime, where no laser modes are active, then Gaussian regime is present.

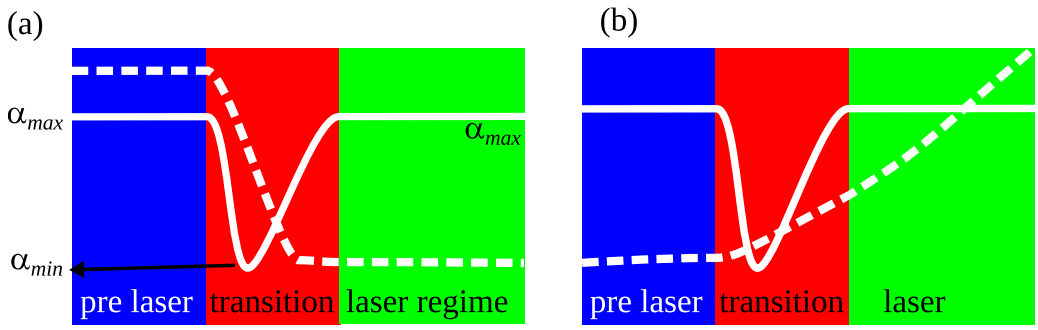

Figure 22 – **Sketch of the expected alpha stable parameter as a function of the pump energy curve**. The alpha values goes from the high value to a minimum in the random laser transition (continuous white curve). The dashed lines represent de FWHM reduction (a) and intensity increases as a function of the random laser regime, below, around and above the laser threshold.

The main idea proposed from Ignesti Reference (68) are:

- If the system has a small mean free path length (compared to the emission wavelength), the system is in the strong scattering regime, thus long path travelled by photons are less probable, as well large intensity fluctuations. If the RL emission occur in such regime, is not probable that the system reaches small α values to

reach a deep Lévy regime. Thus, a RL mode does not retain all the available gain, to dominate the others.

- Large fluctuation can arise as the mean free path length increases, then the system slow comes back to the Gaussian regime, and the width of the *red* region in Figure 22 increases.

Levy statistics was also observed in the Rhodamine 6G based random laser. In Reference (35) the author suggested the Lévy statistic as the universal identifier of RL threshold. Such prediction was analytically derived in Reference (76). A power law probability distribution was obtained and a truncated Lévy like distribution around the threshold described the RL system.

3.2.3 Statistical intensity fluctuations of RL model

In the analysis of Replica Symmetric breaking on random laser, a Hamiltonian with coupling term originated from spatially inhomogeneous refractive index, non-uniform distribution of the gain and an effective damping contribution due to the energy leakage was writen (40) as:

$$H = \sum_{\{jk\}'}^{n} \mathrm{J}_{jk} a_j a_k^* + \frac{1}{2} \sum_{\{j,k,l,m\}'}^{n} \mathrm{J}_{jklm} a_j a_k^* a_l a_m^* \tag{3.3}$$

The Langevin equations for the slow modes amplitudes $a(t)$, with the presence of i.i.d noise, as described in Reference (40) is,

$$\frac{\mathrm{d}a_Z}{\mathrm{d}t} = \frac{\partial H}{\partial a_Z^*} + F_Z, \tag{3.4}$$

with $Z = j, k, l$ and m, describe the intensity fluctuation in random lasers. Writing $I_Z = c_Z |a_Z|^2$ and manipulating the Equation 3.3 leads

$$\frac{1}{c_k}\frac{\mathrm{d}I_k}{\mathrm{d}t} = -2\mathrm{Re}\left\{ \sum_{\{j\}'} \mathrm{J}_{jk} a_j a_k^* + \frac{1}{2} \sum_{\{jlm\}'} \left[\mathrm{J}_{jklm} + \mathrm{J}_{jmlk}\right] a_j a_k^* a_l a_m^* + a_k^* F_k \right\} \tag{3.5}$$

When the authors add the optical noise as a sum of additive and multiplicative statistically independent stochastic processes, and considering slow-amplitude modes $a_Z(t)$, comparing to the rapidly evolving phase dynamics, they obtain the equation for the probability density function (PDF) P of emission intensity I_Z as

$$\frac{\partial P}{\partial t} = -\frac{\partial}{\partial I_Z}\left[(-d_Z I_Z - b_Z I_Z + 2Q I_Z)P\right] + 2Q\frac{\partial^2}{\partial I_Z^2}(I_Z^2 P) \tag{3.6}$$

where Q controls the magnitude of the multiplicative fluctuation, b_Z and d_Z are term that depend on the coupling quartic terms. The solution of Equation 3.6 has a form of a tempered exponential decay power law:

$$P(I_Z) = A_Z I_Z^{-\mu_Z} \exp(-b_Z I_Z/2Q). \tag{3.7}$$

providing a theoretical background that the intensity fluctuations in RLs are governed by a Lévy-like statistics.

In Equation 3.6 the intensities at wavelength indexed by Z are $I_Z > 0$. A_Z is a normalization constant. The solution $P(I_Z)$ with the power law exponent $1 < \mu = 1 + d_Z/2Q < 3$, is described by the Lévy distribution with $\overline{\alpha} = \mu - 1$, that is, an exponentially truncated Lévy distribution of intensities I_Z for $0 < \overline{\alpha} < 2$, for the interval $1 < \mu_k < 3$. The PDF $P(I_Z)$ describes a Gaussian regime $\alpha = 2$ when μ_k is out of the interval $1 < \mu_k < 3$. For a giving disorder strength, the parameter μ_k shifts from an initial Gaussian regime $\mu_k < 1$, to a Lévy-like $1 < \mu_k < 3$ and then goes back Gaussian $\mu_k > 1$. As did Uppu in Reference (35), the author of Reference (40) also proposed the Lévy α-stable parameter as a universal identification of RL threshold. They also proposed, and experimentally demonstrate that the multimode overlap parameter, that describe the Replica Symmetric Breaking in random laser, as these behaviours are described by the same Hamiltonian H, also is a universal identify of RL threshold. In 1D system such behaviour was not well studied, the Reference (77) has proposed that the emission statistic in 1D RL can follow a heavy tailed distribution. In the next section we will show our results of Lévy-like statistic of the intensity fluctuation in quasi-1D RL.

3.3 Our results: Lévy statistic in intensities of random fibre laser

This section study the intensity fluctuation of the output intensity in a continuous-wave-pumped erbium-doped one-dimensional random fibre laser (RFL), with specially designed Bragg grating scatters. The results are published in the Reference (78). Transitions from Gaussian to Lévy-like and back to the Gaussian regime are described as the input excitation power increases from below to above the RFL threshold. Such system presents a large second moment causing an ultra-slow convergence to Gaussian regime. Such experiment demonstrated for the first time the presence of Lévy statistic in one-dimensional random laser system.

3.3.1 Lévy statistic in the intensity fluctuation of a random fibre laser

The device used here was based on a 30 cm Er-doped fibre Bragg Grating, with random phase shifts inserted during the fabrication process. The experimental setup used is shown in Figure 23. A home-assembled semiconductor cw laser operating at

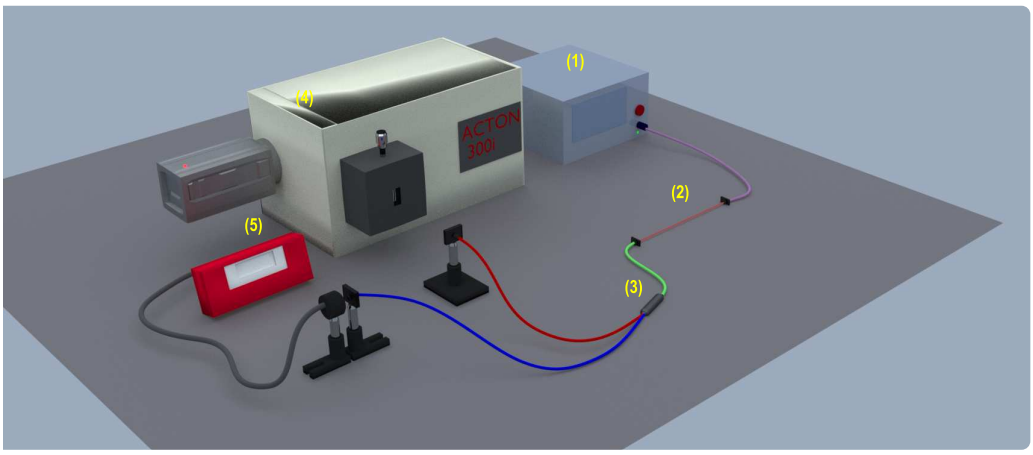

Figure 23 – **Experimental setup used in the intensity fluctuation measurements**. A InGaAs camera (4) with 0.1 nm resolution was used to measure the emission spectrum, the swept time was for measuring each spectrum was 776 ms. A 1480 nm pump (1) diode laser was used to pump the 30 cm Erbium-RFL (2). A wavelength divisor multiplexing (3) was used to split the pump and signal. A power meter (4) monitored the pump power.

1480 nm was used as the pump source. The pump laser was connected to the RFL and the RFL output was split through a 1480 nm/1550 nm WDM. The lower wavelength output was directly pointed to a power meter and the other output to the spectrometer. A liquid-N_2 cooled InGaAs near-infrared camera, spectral resolution of 0.1 nm at 1530 nm, was used to record and save the emission spectra. A collection of 5000 spectra was recorded for each input excitation power, with integration time of 100 ms. This large number of spectra was due the large fluctuation of our RL system if compared to the bulk materials. The intensity fluctuations were measured around the maximum spectral emission intensity, within the spectral resolution of our instrument.

The laser characteristic power in versus power out was again realized. The emitted intensity the Erbium-RFL system for normalized input power below, near and above the threshold are in Figure 24 (a), (b) and (c), respectively.

The estimation of the threshold power was (16.30 ± 0.05) mW determined from the FWHM reduction. Also, the high intensity fluctuation was not related to the pump

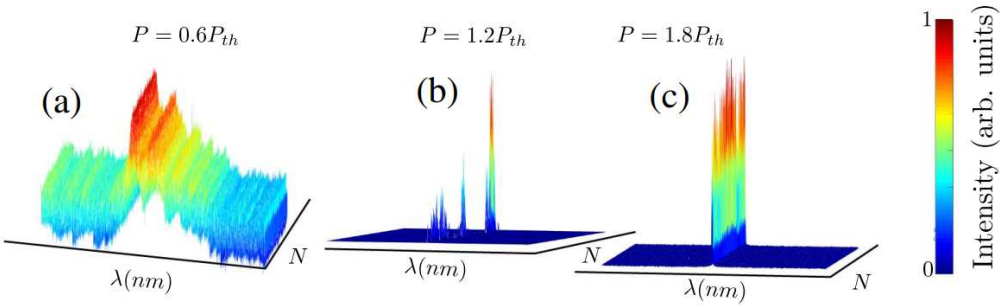

Figure 24 – **Emitted intensity spectra**. Representative emitted intensity for below (a), near (b) and above (c) the RL threshold.

power intensity fluctuation (less than 5%). The pump laser fluctuations do not affect the Erbium-RFL fluctuations, particularly because the former was kept working all the time well above $(10\times)$ the threshold, see chapter 2, and it also agrees with the results of the Reference (44) where the pump and RL signal intensity fluctuation was not correlated. From the experimental data of Figure 24 a discrete sequence of intensities I was obtained and it was used to make the experimental $PDF(I)$

3.3.1.1 Intensity fluctuation

The emitted intensity fluctuation of the 5000 measured spectra are shown in Figure 25 (a-c), and the maximum emitted intensity I of each spectrum evaluated around the laser emission is shown as a function of the recorded label $(1, 2, 3, \cdots, N)$. Observe that such behaviour is clearly similar to the regimes aforementioned, Gaussian (a), Lévy (b), and Gaussian again (c). Thus, a high variance in the intensity fluctuation emission is observed and a Gaussian to non-Gaussian Regime is expected to occur. Figures 25 (d-f) show the experimental histogram of the experimental data shown in (a-c). Two Gaussian-like histogram are shown: below threshold (d) and above threshold (f), also the above threshold regime has more variance than below. The Lévy-like histogram (e) is characterized as an asymmetrically distribution for values larger than the average, because the laser threshold behaviour.

The statistical analysis was done on the probability density distribution $P(I)$ of the maximum emitted intensities. If the second moment of $P(I)$ are finite, then a Gaussian dynamics is assured by the central limit theorem (CLT). If the second moment diverges, e.g., the variance takes large values in relation to the average, the system

dynamics is governed by the Lévy alpha stable distribution, Equation 3.1.

Actually, the Gaussian distribution can be recovered from Equation 3.1 fixing $\alpha = 2$ and taking the location parameter as the mean. So, the Equation 3.1 can describe both Gaussian and non-Gaussian regimes, depending only on the value of the parameter α. The histogram representing the experimental PDF $P(I)$ are depicted in Figure 25 (d-f).

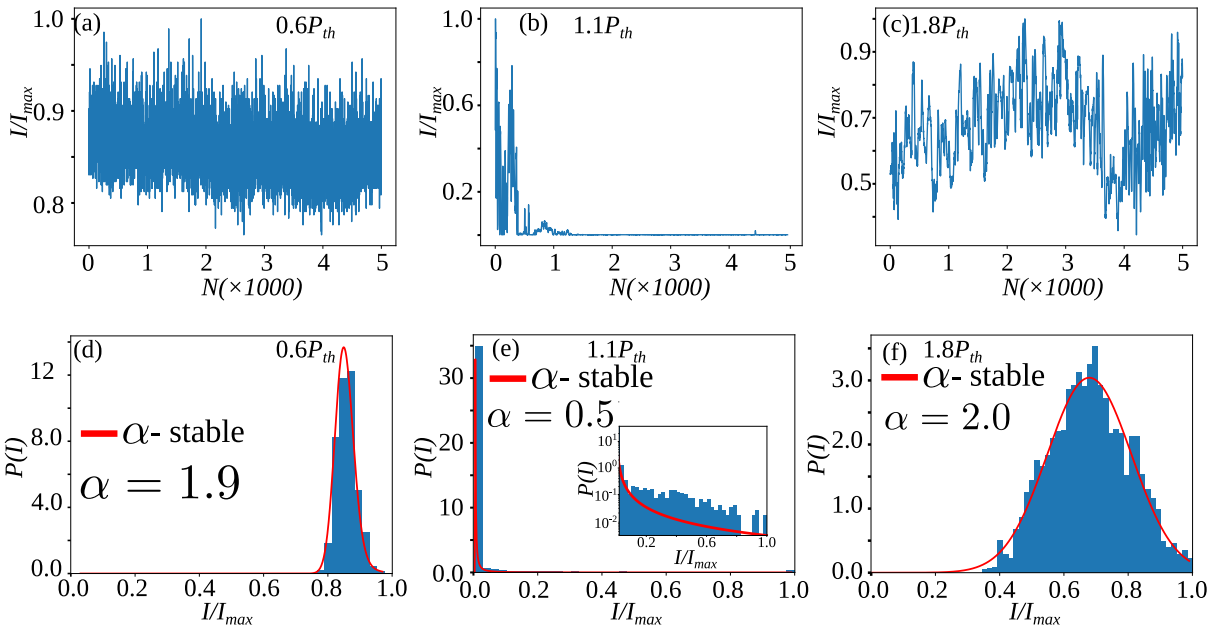

Figure 25 – **Intensity fluctuation and α-stable probability distribution of intensities.** (a-b) Maximum emitted intensity fluctuation from below to above the random laser threshold. (d-e) histogram of the experimental data at the respective relative pump and $\alpha-$stable curve fit using the quantile method provided by scipy.

Such results are supported by the theoretical summary presented in the previous sections. Where are included: the gain and radiation loss; the disorder mechanisms with a background spatially inhomogeneous refractive index; non-uniform distribution of the gain, and cavity leakage.

The Experimental PDF $P(I)$, shown in Figures 25 (d-f) by the histogram, has the best fit to Equation 3.1 represented by continuous red curve. The parameters were estimated using the fast quantile-based method (79) implemented in an open-source library [1] that also provides the probability density function calculations (74).

[1] The quantile-based method in such library is used only to find the starting points that are used in other methods but, the quantile precision is acceptable when used with caution. To access the

Observe that the α values are consistent with the fluctuation observed. The Gaussian regime below and above for $\alpha \approx 2$, Figure 25 (d) and (f) and a Lévy like distribution with $\alpha \approx 0.5$, Figure 25 (e). The obtained stable parameter values are in table 2. The positiveness asymmetry of the intensities is represented by $\beta = 1$. The location parameter v agrees with the intensity where the histogram, Figures 25 (d) and (f), shows it maximum, and in the Gaussian regime with the mean values. A wide spread of intensities is observed by the broadening of the PDF $P(I)$ from below to above the threshold. It is related to the intensity fluctuation above the threshold larger than below, but much weaker than those observed near the threshold.

Table 2 – Summary of the Best Fit Parameters to Equation 3.1 for the measured intensity PDFs of Figs. 25 (e-f)

Input power	α	β	v	c
$0.6P_{th}$	1.9	1.0	0.858	0.021
$1.1P_{th}$	0.5	1.0	0.001	6.25×10^{-5}
$0.8P_{th}$	2.0	1.0	0.682	0.682

The confirmation of the Lévy-like behaviour of the measured emitted intensities of the 1D Erbium-RFL system is shown in Figure 26. The main parameter of the α-stable distribution is in function of the normalized input power P/P_{th}. With the increases of P/P_{th} the statistics of intensities fast goes from pre-lasing Gaussian ($\alpha = 2$) to the Lévy like ($0 < \alpha < 2$) behaviour around the RL threshold. And then, when $P/P_{th} > 1$, the statistics return again to a new Gaussian Regime, but now it is in the RL phase, with less fluctuation than around threshold but more fluctuation than below threshold. It is the same behaviour observed in bulk random laser (29, 35, 76) and the observed independence on dimensionality here is also supported by the Langevin treatment aforementioned. Also, the curve clearly coincides with the linewidth reduction, as suggest by (35), it reinforces that the Lévy behaviour is an identifier of the RLs threshold, e.g., a fast decay on the FWHM values is observed when the system reaches the non-Gaussian regime.

This change in the statistical regime can be viewed as a result of the change in the homogeneity of the gain distribution as the pump power P increases relatively to the threshold power P_{th}. Near the pump energy threshold, a given mode can dominate

quantile method is necessary to use `_fitstart(lista_max)` that can be founded in the source code of scipy library (80).

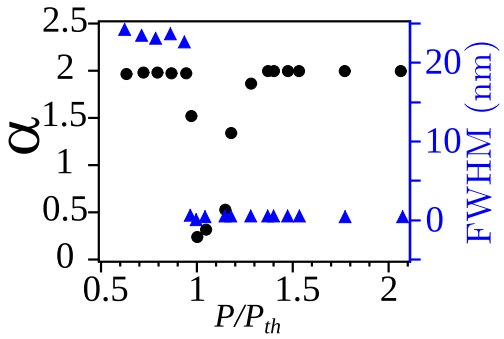

Figure 26 – **Lévy stable distribution parameter α (circles) and FWHM (triangles) as a function of the normalized input power**. The evolution of the α values with the increases of the pump power shows three statistical regimes of intensity fluctuations for the Erbium-RFL system: pre-lasing Gaussian $\alpha \approx 2$ regime, Lévy RL emission $0 < \alpha < 2$ around the threshold P_{th}, and Gaussian RL behaviour of the emitted intensities $\alpha \approx 2$ above the threshold P_{th}. The sharp decrease in the α values at the first Gaussian to Lévy transition coincides with the abrupt change in FWHM at the RL threshold.

over the others taking the highest amount of the gain with a large gain path. Large fluctuation arises from relevant fluctuation in photon path length. Raising the probability of extreme events characteristic of heavy-tailed power law Lévy distribution.

3.3.1.2 Lévy statistic and spin glass behaviour

In the previous chapter we introduced the glass treatment of RLs. The effective Hamiltonian

$$H = \sum_{\{jk\}'}^{n} \mathrm{J}_{jk} a_j a_k^* + \frac{1}{2} \sum_{\{j,k,l,m\}'}^{n} \mathrm{J}_{jklm} a_j a_k^* a_l a_m^* \tag{3.8}$$

is expressed with the amplitude of the normal modes. The disorder is included in the sum of the quadratic and quartic term, both possess the same origin on the systems disorders. Such Hamiltonian is analogue to the Hamiltonian of disorder spin glass model (38). With the pump power being the role of the inverse temperature, and the modes amplitudes like spin variables. A phase diagram of RLs was constructed based on this Hamiltonian, and the modes as a function of the input power and disorder strength determines the photonics phases (64).

The replica symmetric breaking characterization is made by the distribution of the mode-to-mode correlation parameter for many system replicas. The paramagnetic scenario is when the distribution of the parameters is centred at zero. But when the distribution has peaks at non-zero values, the symmetry of the system is broken, and spin

glass phase emerges. The order parameter can be calculated by the correlation of the modes, or by the emitted intensity. Using the intensity, more experimental accessible, the order parameter is given by

$$q_{\gamma\beta} = \frac{\sum_k \Delta_\gamma(k)\Delta_\beta(k)}{\sqrt{\sum_k \Delta_\gamma^2(k)}\sqrt{\sum_k \Delta_\beta^2(k)}} \tag{3.9}$$

where γ,β = 1, 2,...,N_S, with $N_S = 5000$ for each pump power, denote the replica labels, the average intensity at the wavelength indexed by k reads $\overline{I}(k) = \sum_{\gamma=1}^{N_S} I_\gamma(k)/N_S$, and the intensity fluctuation is given by $\Delta_\gamma(k) = I_\gamma(k) - \overline{I}(k)$. The same experimental data used to analysis the intensity fluctuations are applied in the spin glass analyse. Figure 27 show q_{max} values as a function of the relative input power P/P_{th}. A RSB phase transition can be observed with a sharp transition from $|q| = 0$ to $|q| > 0$ values, signalizing the presence of the RL glass phase transition. In the same Figure are also present the characterization of the intensity statistic by the Lévy $\alpha-$stable distribution.

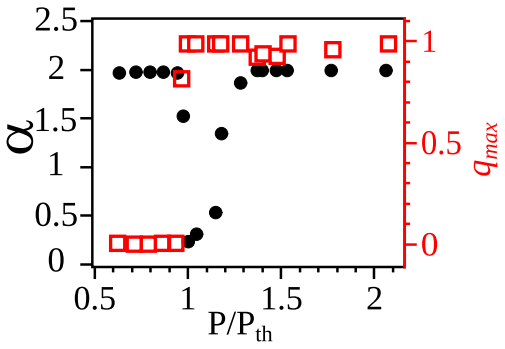

Figure 27 – **Lévy stable distribution parameter α (circles) and RL glass behaviour determined by the order parameter q as a function of the normalized input power**. The evolution of the α values with the increases of the pump power shows three statistical regimes of intensity fluctuations for the Erbium-RFL system: pre-lasing Gaussian $\alpha \approx 2$ regime, Lévy RL emission $0 < \alpha < 2$ around the threshold P_{th}, and Gaussian RL behaviour of the emitted intensities $\alpha \approx 2$ above the threshold P_{th}. The sharp decrease in the α values at the first Gaussian to Lévy transition coincides with the RL glass phase transition.

Figure 27 shows that Lévy-like behaviour and spin glass transition occur simultaneously at the RL threshold. This behaviour was first reported in bulk random laser, now was also demonstrated in low dimension RL system. Both behaviours can be theoretical supported by the Langevin equation of the normal modes with the same Hamiltonian, and maybe have the same physical origins. A complete explanation is still

an open task (68). This results also proposed that the presence of extreme events in low dimensional random laser can be present. Actually, in the next chapter, the application of the Generalized extreme events statistics in random fibre laser is made.

4 EXTREME EVENTS

Extreme events mean the presence of independent identical distributed variable of large values, in other words, the presence of an extreme high value event of low probability. With large number N of an event realization, if p is the probability of occurrence of a determined event, the amount of times that it can appear goes with Np, a rare event of probability $1/N$ can occur at least one time (81). In nature, the occurrence of extreme events is also present. Rogue waves, giant sea waves that rarely occur, with step much larger than the neighbour waves level, is a known example. Extreme events also impacts the market management (82, 83), and the measurement of the energy that hit the earth from solar wind (84), are examples.

4.1 Examples in optics

The rogue waves concept in optics was introduced using soliton propagation in microstructured optical fibre, where huge light waves arises from smooth pulses that are perturbed by low intensity noise (85). This rare emission events in supercontinuous pulse generations was demonstrated that can be enhanced using a proper modulation of the pump pulses envelope, with an order of magnitude higher, in the generation rate of such extreme events, and a slide frequency can diminish this rate (86).

Rogue waves were also observed by Hammani in Raman amplification, using commercial high non-liner optical fibres due an increased spectral broadening (87). They also proposed that a partially incoherent pump can lead to exhibition of Rogue waves (88).

4.1.1 Extreme statistic in random laser

In optics, random fibre laser is a wealthy device to explore extreme events as results of their complex behaviour as well offer more control over the experiment. Gorbunov et al. (89) studied the intensity dynamics of a half open cavity laser. The system used was a 40 km single mode fibre (SMF28) directly pumped by a 1445 nm Raman fibre laser and coupled to a FBG with λ_B =1550.5 nm. This complex system has the gain provided by stimulated Raman scattering, and feedback by the Rayleigh

scattering due to refractive index fluctuation. It was observed a stochastic behaviour of the intensity of the emitted spectra, with the intensity like identically distributed random variable with a large sequence of measurements $N >> 1$. Strong intensity fluctuation was observed, and occurrence probability diminish with the pump power increases. Indeed, the intensity dynamics show large events, at least 20 times larger than the average value (89).

In bulk random laser the statistics of extreme have been studied by Uppu (90), observing its dependence on the pump power and scatter strength. Large intensities were again most possible to occur at low pump power, where gain is scarce and some photons modes can dominate over the others. Large pump power makes that large intensity being not rare, and extreme events probability are very reduced. However, the use of GEV distribution to characterize the random laser emission dynamics was performed only in (90), and a possible connection between the Lévy $\alpha-$stable distribution of random laser intensities was proposed.

The asymptotic study of extreme values of independent and identically distributed random variables is given by extreme value theory. For any PDF $P(I)$ of N random variables forming a set of I values, such that $I \in \{I_1, I_2, \cdots, I_{N-1}, I_N\}$, the cumulative distribution function of the maxima $F_{max}(x)$, where $x = \max\{I_1, I_2, \cdots, I_{N-1}, I_N\}$, in the limit where the number of samples $N \to \infty$, has a limit distribution that belongs to one of standard type of extreme value distribution (81). The three independent distribution are (73)

- Gumbel distribution, that join all PDF $P(I)$ with a tail falling faster than a power law, that is, PDF that goes to Gaussian distribution in the central limit theorem, and present no upper bounds. The distribution F of their maximum x is given by:

$$F_{Gumbel}(x) = \exp\left[-e^{-\frac{x-m}{\sigma}}\right],\ x \in \Re. \tag{4.1}$$

- Fréchet distribution includes PDF $P(I)$ with a tail falling as a power law and in the central limit theorem not recover a Gaussian distribution. Has $P(I) \sim I^{-\mu}$, in the limit $N \to +\infty$, and $\xi = \frac{1}{\mu-1}$. This distribution also has no upper bounds limit, and $F(x)$ is:

$$F_{\textit{Fréchet}}(x) = \exp\left[-\frac{1}{\left[1+\xi\left(\frac{x-m}{\sigma}\right)\right]^{1/\xi}}\right],\ x \in [m-\sigma/\xi, \infty],\ \xi > 0; \tag{4.2}$$

- Weibull distribution are PDF that has a finite right endpoint, x^*, where the F fast goes to 1.0,

$$F_{Weibull}(x) = \exp\left[-\left(\frac{m+(\sigma/|\xi|)-x}{\sigma}\right)^{1/\xi}\right],\ x \in [\infty, m+\sigma/\xi],\ \xi < 0; \qquad (4.3)$$

A distribution that gather the three extreme values distribution is the Generalized Extreme Values distribution (GEV). Similar to the case of α-stable distribution where only a parameter describes the regime, Gaussian or Lévy, in the GEV distribution that reads as,

$$F_{\xi,m,\sigma}(x) = \exp\left[-\left(1+\xi\frac{x-m}{\sigma}\right)^{-1/\xi}\right] \qquad (4.4)$$

the main shape parameter $\xi \in (-\infty, +\infty)$ describes the class of extreme events the CDF $F(x)$ is, Gumbell $\xi \to 0$ or Fréchet (Weibull) $\xi > 0$ ($\xi < 0$). And the parameter $m \in (-\infty, +\infty)$ is the location, $\sigma > 0$ is the scale parameter and $1 + \xi\left(\frac{x-m}{\sigma}\right) > 0$.

The value of the main parameter ξ influences over the shape of the distribution is shown in Figure 28 where three values of ξ is used. In (a) and (b) are PDF $P_{max}(x)$, and (c) and (d) show the distribution $F(x)$. The function has x values limited by the percentiles of percent 0.01 and 0.99 (a-c).

When $\xi = -0.5$ (blue dotted curve) a right upper bound is present, Weibull case, and a minimum limit is not present, and F fast converges. In the other side, for $\xi = 0.5$, the Fréchet distribution is recovered and it has no upper bound and slow converges (c). Finally, for $\xi \to 0$, the distribution fall fast, no upper bound is present. The scale and location parameter used to obtain these curves are 1.0 and 0, respectively.

4.1.2 Lévy distribution and extreme events

The Lévy $\alpha-$stable distribution has the characteristic function given by

$$\overline{P}(k) = \exp\{ikv - |ck|^{\alpha}[1 - i\beta\mathrm{sgn}(k)\Phi]\} \qquad (4.5)$$

The main parameter α determines if the regimes are a Gaussian $\alpha = 2$ or Lévy like $0 < \alpha < 2$. As intensities' fluctuation in random laser increases, the α decreases and the system has a PDF, of intensities I, $P(I)$ with a fat tail. As mentioned in the previous chapter, the intensity dynamics of random laser follows a power law behaviour, with PDF $P(I) \sim I^{-\mu}$. It includes the regime where $P(I)$ decay at large I faster than a power

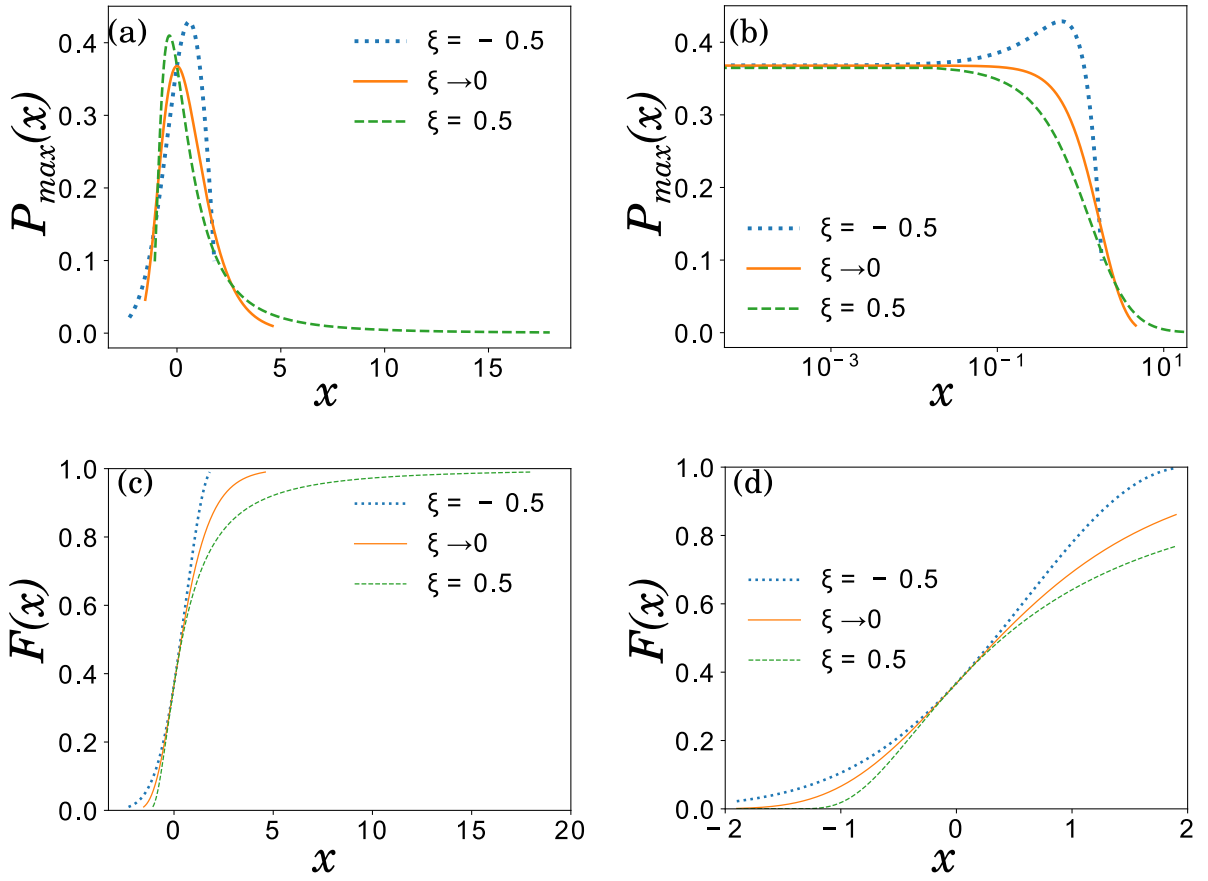

Figure 28 – **Generalized extreme value distribution examples.** PDF $P_{max}(x)$ with the curves limited by the percentiles of percent 0.01 and 0.99. Convergence is show by the cumulative function $F(x)$ (c-d).

law, $\mu \geq 3$, resembling the $\alpha = 2$ Gaussian statistics. The Lévy like PDF is recovered for heavy tailed power laws with large second moments, with $\alpha = \mu - 1$. It is expected that if dynamics of the emitted intensities of RL has its extreme value statistic governed by the Fréchet domain, $\xi > 0$ in the GEV distribution, a connection between the Lévy $\alpha-$stable and GEV distribution of the RL emitted intensity is also present, $\xi \sim 1/\alpha$. This feature was not observed it in Reference (90) due the low number variables. One should expect that $\alpha = \mu - 1 = 1/\xi < 2$ if the parameter $\xi > 1/2$, the Lévy regime is present. Or $\alpha = 2$ if $0 < \xi \leq 1/2$, the Gaussian Regime govern the system. If $\xi \to 0$, a distribution that fall faster than a power law is expected, $\alpha = 2$ Gaussian distribution.

4.2 Our results: Extreme statistics applied in random fibre laser

In this section we report our observation of extreme intensity events in a quasi-one-dimensional cw-pumped Erbium doped random fibre laser. The results were also

published in Reference (91). The same device employed to the Lévy study and first characterized in the Reference (49) is used here. But, for the statistical analyses a very large number of emitted spectra was collected (150000), $30\times$ more than the amount collect in (90).

The experimental setup used is the same used to the Lévy-like behaviour study present in Figure 23 and described in the last chapter, with each spectrum being record with integration time of 50 ms.

The intensity value at the wavelength of maximum output intensity of the measured spectrum j is denoted as I_j, forming a long-time series sequence $\{I_j\}$, with $j = 1, 2, ..., N$, $N = 150000$ for each excitation power. The total time measurement was $\approx$ 150 min. The random phase shifts inserted in the Bragg gratings makes a stochastic intensity dynamic as a result of the system disorder, that are present in the Langevin equation from where the PDF $P(I)$ can be determined (40).

To obtain the set of x maximum values, we subdivided the sequence $\{I_j\}$ into M blocks of N/M intensity values each, such that $M >> 1$ and also $N/M >> 1$. A new long-time series x_n was generated at each excitation power, with $n = 1, 2, ..., M$, where x_n is the maximum intensity among the values of the nth block of N/M intensities. The experimental distribution of the extreme values is determined by $\{x_n\}$, with PDF given by $P_{max}(x)$, and cumulative density function (CDF) $F(x) = \int_0^x P_{max}(x)dx$. The choice of number of spectra blocks (M) and the number of intensities (N/M) in each block can reflect on the fits parameter of the GEV distribution (84). If a large number of intensities per block (N/M) is chosen, this rise to a small number of M blocks, e.g., low number of maxima values $x = M$, making the experimental CDF $F(x)$ not statistically significant. And the contrary, with a large number of maxima x and low number of spectra per block, can reflect on a statistical irrelevancy on the maxima per block. As N is fixed (150000), the choice was made such that $N >> 1$ and $N/M >> 1$.

It is expected that the statistic of the emitted intensity of the random fibre laser can change as the input power increases. The Gaussian to Lévy, and back to Gaussian transition is observed around the threshold value, as mentioned in the last sections. The Lévy domain have their statistic of their maxima describe by the Fréchet distribution (GEV distribution with the shape parameter $\xi = (\mu - 1)^{-1} > 1/2$).

The emitted intensities at the wavelength of maximum emission intensity of the

Erbium-RFL, forming the set of $\{I_j\}$ discrete values of the spectra $j = 1, 2, ..., N$ $(N = 150000)$, are described in Figure 29. The normalized excitation power chosen was (a) $P = 0.77P_{th}$ well below the threshold, (b) $P = 0.88P_{th}$ near and below the threshold, (c) $P = 1.21P_{th}$ near and above the threshold, and (d) $P = 1.72P_{th}$ far above the threshold of the random laser.

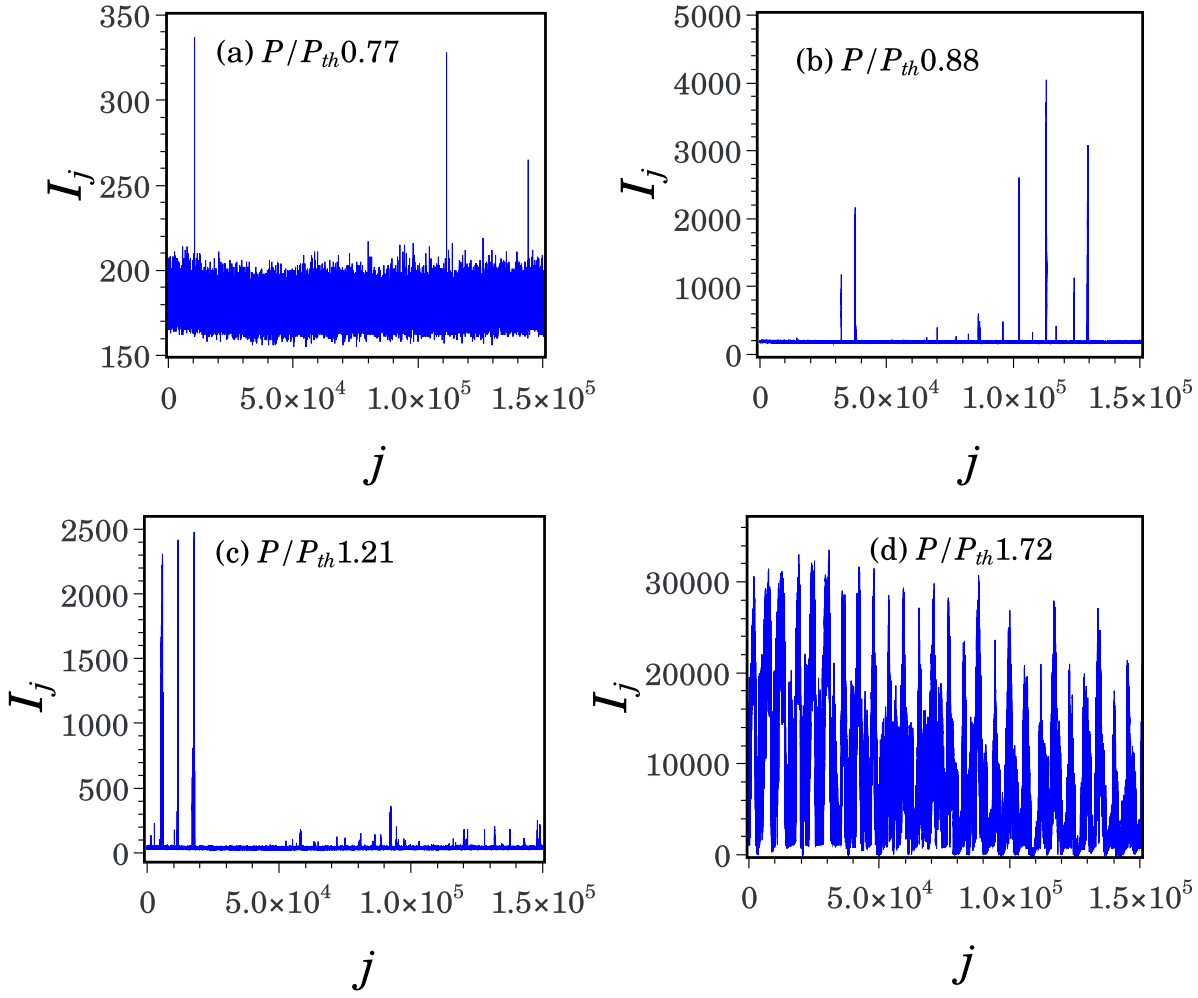

Figure 29 – **Maximum intensity value I_j (in arbitrary units) of the spectra $j = 1, 2, ..., N$ (=150,000) emitted by the Erbium-RFL system**. Data are shown for four values of the normalized excitation power 0.88P_{th}, (c) 1.21P_{th}, and (d) 1.72P_{th}. The threshold power was P_{th} = 16.30 mW.

It is observed that a drastic change in the fluctuation patterns of $\{I_j\}$ appears as the threshold is reached. In both regimes near the threshold has a fluctuation up to $\sim 22\times$ (b) and $\sim 66\times$ (c) above the average intensities. And it maximum appear not so often. The fluctuation well above (d) and below (a) the threshold does not present any rare event of large peak intensities (actually the few peaks intensities that appear in (a)

are not laser emission).

The sequence of maxima $\{x_n\}$, with $n = 1, 2, \cdots, M$, obtained by subdividing the set $\{I_j\}$ into $M = 800$ blocks of 187 intensity values each, with the maximum value of block n denoted as x are depicted on Figure 30. The pattern of the new variables x is observed to be similar to those of Figure 29.

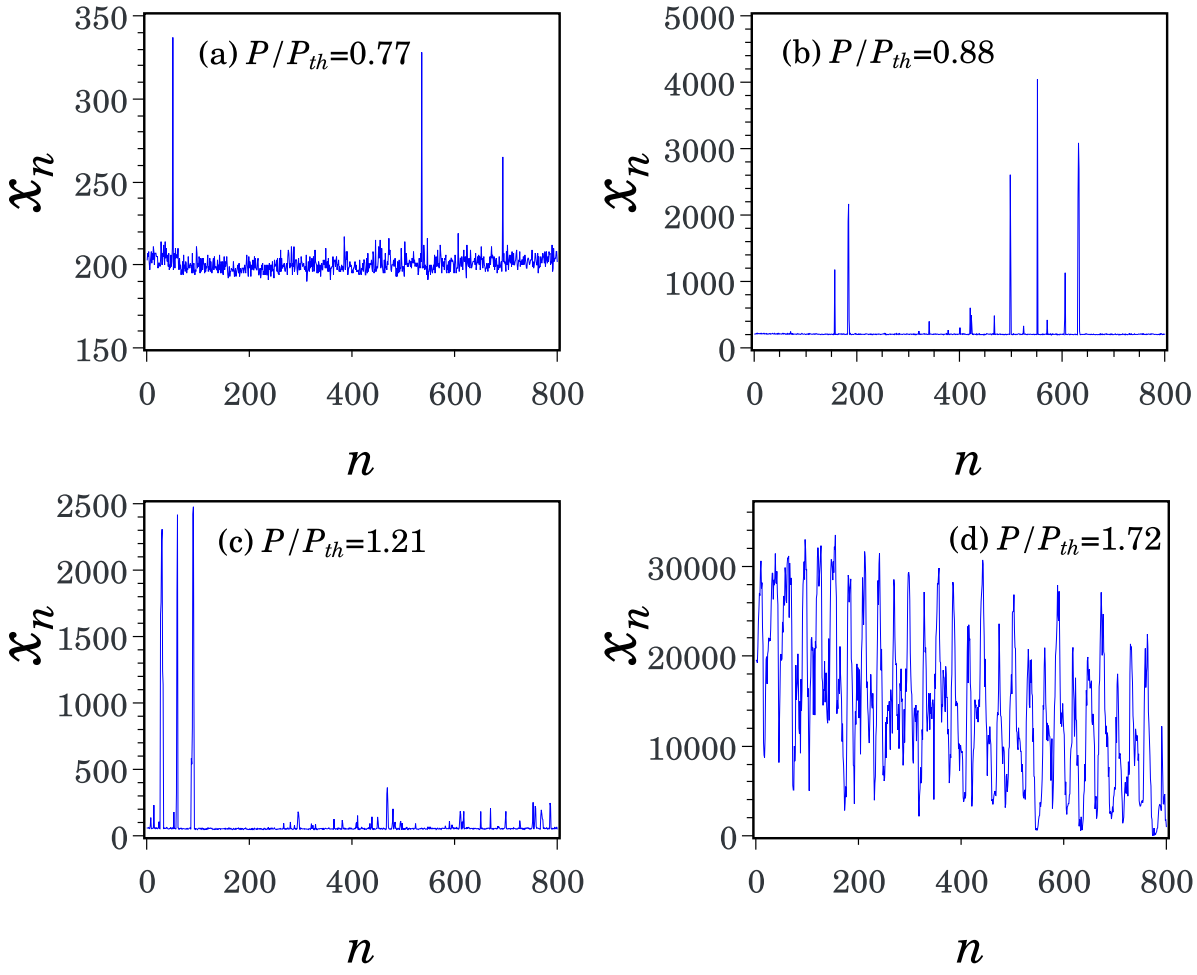

Figure 30 – **Maximum intensity value x_n (in arbitrary units) for each box n.** Data are shown for four values of the normalized excitation power 0.88P_{th}, (c) 1.21P_{th}, and (d) 1.72P_{th}. The threshold power was P_{th} = 16.30 mW.

The increase in the magnitude of intensity fluctuations observed near the threshold in Figs. 29 and 30 suggests that the PDF of intensity values $P(I)$ can be generally described by the family of Lévy αstable distributions. Indeed, in agreement with previous statistical regime mentioned in the Lévy section aforementioned, if $0 < \alpha < 2$ and the Gaussian limit if $\alpha = 2$, and report in other works (29, 40), by the determination of the best-fit parameters of the experimental PDF $P(I)$ to the Fourier transform of α stable function, a Gaussian regime was readily identified well below the threshold, with

the Gaussian value $\alpha = 1.98$ at the pump power $0.77P_{th}$. For well above the threshold, the best fit was obtained by the exponential, the best fit obtained well above threshold at pump power of $1.72P_{th}$ also assures that the PDF $P(I)$ is governed by the $\alpha = 2$ Gaussian statistics according to the CLT. However, such Gaussian regime present important differences since, for instance, the former, below threshold, corresponds to the pre-laser behaviour, whereas the latter, above threshold, has been characterized as a random laser regime where a self-averaging of the gain between the active laser modes is present.

In contrast to these Gaussian regimes observed far from the threshold, the Lévy statistical behaviour is clearly identified just above the threshold, with the best-fit value α =1.69 determined at P/P_{th} = 1.21. We mention that even lower values of α can be found when the threshold is approached from above, as reported as showed in our last results. However, for excitation powers very close to the threshold the intensity fluctuates so widely that relatively stable results for the EVS analysis in this regime would require the collection of a much larger number of emission spectra.

In the pump power near below the threshold $0.88P_{th}$, the fluctuation pattern is distinct of the well below the threshold $0.77P_{th}$. As laser modes starting to be activated the system are in the boundary between the Gaussian and Lévy regime, the Lévy stable parameter best fit was α =1.88. As proposed experimentally in other works (68) the system can still be considered as in the Gaussian regime for $\alpha > 1.80$. The issue to determining precisely the Lévy index α from the analysis of the PDF of intensities in random laser systems is a not easy task, another approach as proposed in Reference (92), where intensities fluctuations not easy to detect by the Lévy analysis can be detected. Even with more intensity fluctuation than the well below the threshold, the system is still under a regime where it PDF $P(I)$ is Gaussian in the CLT for far above the threshold.

Figure 30 shows the experimental PDF $P(I)$ for the same data of the Figure 29, normalized by the maximum value in the set $\{I_j\}$ (I/I_{max}), the red circles are the experimental results and the dashed curve is the best fit adjust. Observe that in the case far above the threshold, an exponential fit was the most snuggled.

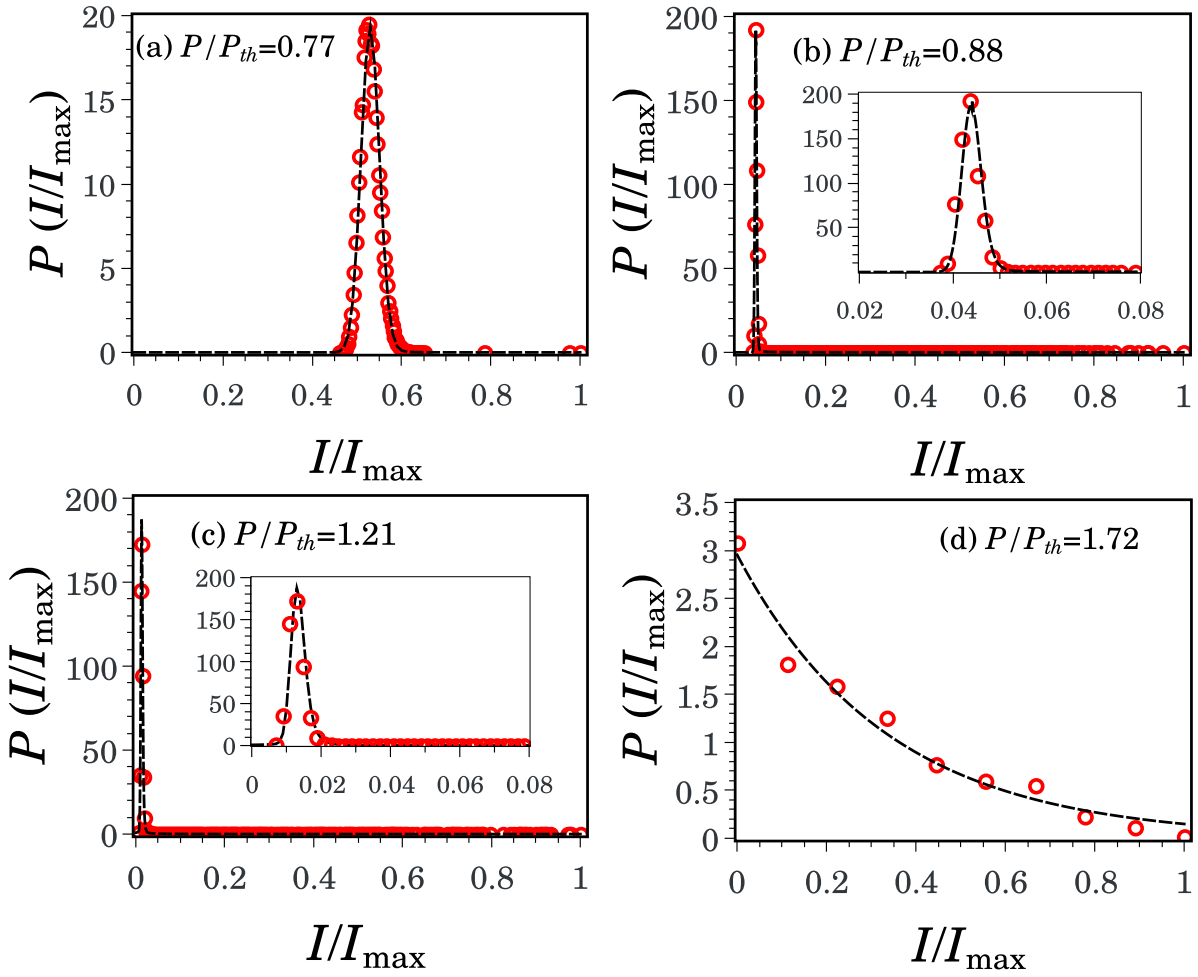

Figure 31 – **PDF $P(I)$ of the emitted of the set of intensities $\{I_j\}$ of the Figure 30**. The red circles are the experimental points and dashed lines indicate the best-fit curves to Lévy α-stable distribution (a-c), and an exponential fit emerges in (d). Gaussian statistic is observed in the pump power below (a,b) and for pump power far above the threshold we can infer a Gaussian regime as result of the CTL (d), according to the central limit theorem. The Lévy distribution $\alpha = 1.69$ is near above the threshold (c), The intensities are normalized by the maximum emitted intensity I_{max} between the 150,000 spectra.

4.2.1 Extreme events fit of the experimental CDF

From the data of the Figure 30 the experimental CDF $F(x)$ is determined for each pump power, with the results depicted as green circles in Figure 32. The curves, solid red line and dashed blue line, represent respectively the Gumbel and GEV best fit. For the Gaussian regime well below the threshold $0.77P_{th}$, both fits are similar, that indicates the $\xi \to 0$, that the GEV fit can be well approximated by the Gumbel distribution. The GEV shape parameter obtained was $\xi = 0.08$. The best fit of the shape

parameter is typical of a large-I power-law PDF $P(I)$ with exponent, as aforementioned, $\mu = 1 + 1/\xi = 13.4 > 3$. Indicating of a Gaussian behaviour of intensity fluctuation with $\overline{\alpha} = 2$, since $0 < \xi \leq 0.5$. Also, this agrees with the $\alpha = 1.98$ obtained directly from the PDF $P(I)$.

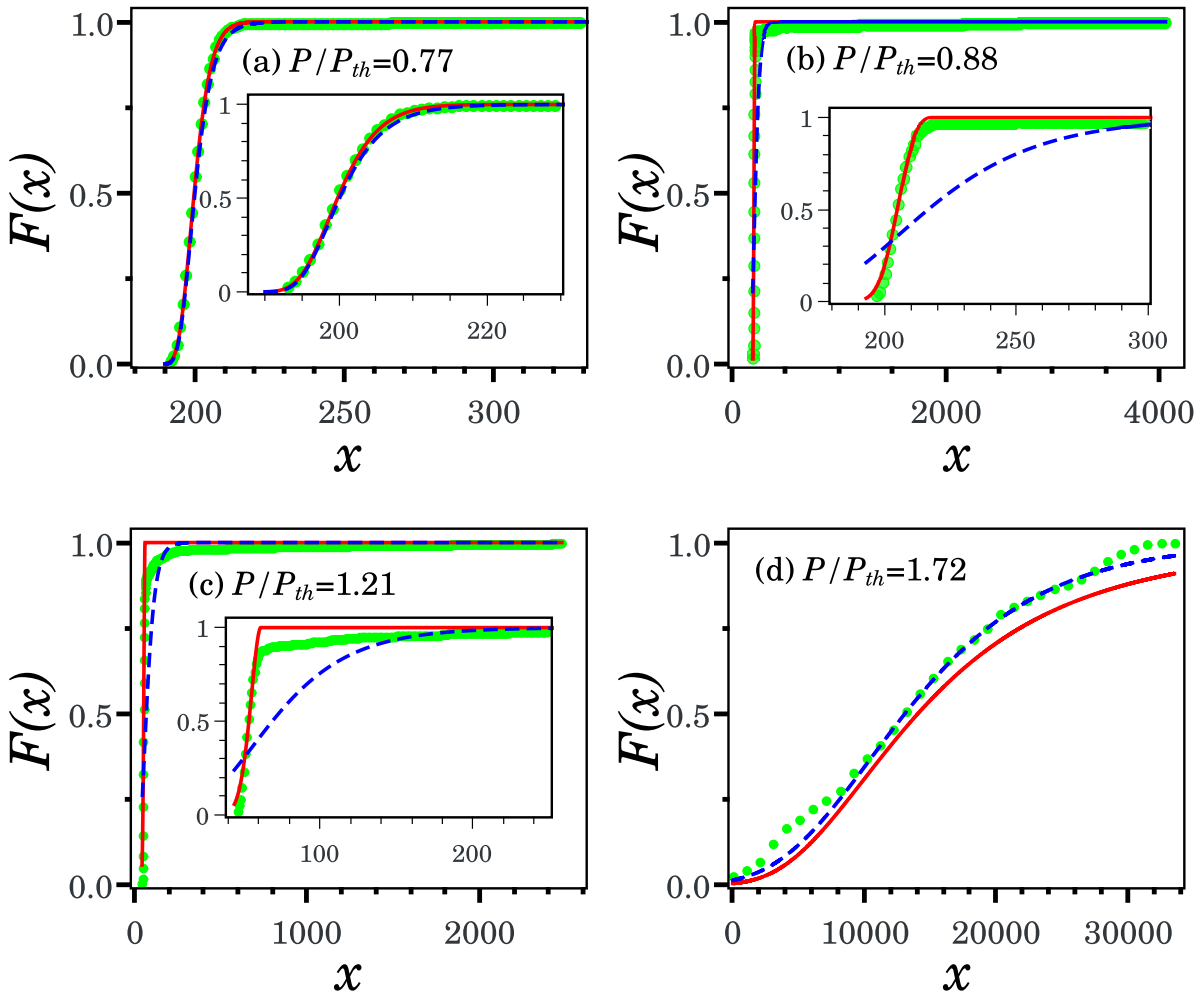

Figure 32 – **Experimental CDF of maxima and the GEV fits**. Experimental cumulative distribution from the analysis of the $\{x_n\}$ as green circles. The best fit curves to the Gumbel are indicated as solid blue and dashed lines. The GEV best fit are continuous red lines. The Fréchet regime is obtained for the pump power near the laser threshold with the shape parameter ξ consistently with the Lévy statistical behaviour of the PDF $P(I)$.

For the case near but below the threshold, $0.88P_{th}$, the intensity fluctuation increases, as observed in Figures 29 and 30, as the system is in the pre-laser regime. In the results of the Figure 32, the CDF $F(x)$ is well fitted to the Fréchet distribution for $0.88P_{th}$. The best fit shape parameter is $\xi = 0.35$ for this case it makes that the associated power law parameter $\overline{\alpha}$ falls with $\mu = 1 + 1/\xi = 3.86$ more slowly that in the

well below threshold regime ($\mu = 13.5$), but it is still on the Gaussian regime according to the CLT. And is very close to the Gaussian boundary value ($\mu = 3$), signalizing to the proximity of occurrence of the threshold. The outlier emission peaks observed at this pump power are not well characterized by the $\alpha-$stable distribution, the attempt to indicate that the system changes in a certain time window from Gaussian to Lévy was in (93) as a result of the photon path fluctuation, but the number of intensities collect must be larger than $150,000$ to have a well statistical significance.

In the Lévy regime for pump power just above the threshold with $1.21P_{th}$ the GEV distribution for $\xi = 0.62$ provides better fit than the Gumbel to the experimental CDF $F(x)$. The best-fit shape parameter implies to a power-law exponent $\mu = 1+1/\xi = 2.61$, that is below the boundary $\mu < 3$, indicating a $P(I)$ with a large$-I$ asymptotic dependence of $P(I)$, and $\alpha = 1/\xi = 1.61$ which is similar to the $\alpha = 1.69$ resulting from the direct analysis of the PDF $P(I)$ of intensities. In the case far above the threshold, the self-averaged gain makes that extreme events being rare, the shape parameter $\xi \to 0$. It implies that $\overline{\alpha} = 2$. It indicated that the PDF $P(I)$ falls faster than a power law, which is consistently to the exponential fit, that can recover a Gaussian behaviour in the CLT.

5 FINAL REMARKS

We mounted and characterized an Er-RFL system which employs a specially designed FBG, and a typical laser threshold and spectral narrowing were characterized. Using speckle contrast we showed that the Er-RFL has a multimode behaviour, showing that this system can be used as light source for image acquisition by the measured low speckle contrast.

We apply our system to study statistical phenomena as a photonic platform. With the analogy to spin glass system, we observed the glassy behaviour in one dimensional RFL. The order parameter q for the intensity fluctuation overlap, was calculated from the experimental data and the RSB phase transition signalized by the change on the shape of the PDF $P(q)$ was observed. This results can contribute to understand the laser behaviour in random media with the thermodynamic background. Also, more study on the connection of spin glass phase and heavy tail intensity distribution are still necessary in other kinds of random media, and with different gain mechanism.

With the analysis of the fluctuation of the laser emission intensity, we demonstrated for the first time that their statistical regimes of intensity fluctuations in a one-dimensional RL system, shifts from the pre-laser Gaussian to the Lévy-like behaviour around the threshold, and to the subsequent Gaussian regime above the threshold. Gaussian to Lévy transition coinciding with the RL threshold, as suggested by other authors, was confirmed. Such transition also indicates the boundary between the photonic paramagnetic regime to spin glass transition in RL. Our results are consistent with the theoretical analysis based on Langevin equation (40, 76).

As the laser action starts, the interplay between the gain and feedback due to the large number of disordered scatterers, changes the output intensity statistics as the injected pump power increases. Such mechanism are also present in the quadratic and quartic term of the Langevin equation. The complexity of the laser build up in a strong scattering medium (large number of random phase shifts in a unique FBG), result in strong intensity fluctuations emerging around the threshold value that can give rise, as demonstrated, to extreme events of statistical significance.

We reported, for the first time, the observation of intensity extreme events in

one-dimensional RFL. A large number of emission spectra was analysed in the regimes below (far and near) and above (near and far) the random laser threshold. The intensity GEV statistic of the experimental data complies nicely with the theoretical predictions based on the stable GEV distributions, with Gumbel and Fréchet distribution for the regimes far and near the threshold, respectively. A good agreement between the Lévy statistics and Gaussian was also observed, showing that RL are good platform for demonstration of statistical predictions. Depending on the excitation power the extreme events of emitted intensities are well described by the Gumbel distribution, with a PDF $P(I)$ that fall faster than a power law (Gaussian Regime below the threshold), or by the Fréchet distribution, with a PDF that resembles a fat tail distribution.

We expect that our results can introduces new insights in the random laser phenomenology. Further work on complex system using the Er-RFL platform can be realized. Our group is already studying the relationship betweens turbulence and spin glasses (94). Random bit generation can also profit from RLs, as already demonstrated in bulk (95) and in fibre RLs (96).

6 PUBLICATIONS

6.1 Publications with the results of this thesis

1. A. S. L. GOMES, et al. Glassy behavior in a one-dimensional continuous-wave erbium-doped random fiber laser. *Physical Review A*, v. 94, 07 2016.

2. B. C. LIMA, et al. Extreme-value statistics of intensities in a cw-pumped random fiber laser. *Phys. Rev. A*, American Physical Society, v. 96, p. 013834, Jul 2017.

3. B. C. LIMA, et al. Observation of Lévy statistics in one-dimensional erbium-based random fiber laser. *J. Opt. Soc. Am. B*, OSA, v. 34, n. 2, p. 293–299, Feb. 2017.

6.2 Other publications

4. E. P. Raposo, et al. Evidence of a Floquet Phase in a Photonic System. *Physical Review Letters* 122, 143903, 2019.

5. I. R. R. González, et al. Turbulence hierarchy in a random fibre laser. *Nature communications* 8, 15731, 2017.

6. B. C. Lima, et al. Plasmon-Assisted Efficiency Enhancement of Eu3+-Doped Tellurite Glass-Covered Solar Cells. *Journal of Electronic Materials* 46 (12), 6750-6755, 2017.

7. L. A. Florêncio, et al. Efficiency enhancement in solar cells using photon down-conversion in Tb/Yb-doped tellurite glass. *Solar Energy Materials and Solar Cells* 157, 468-475, 2016.

8. E. P. Raposo, et al. Universal Phase Transitions in Random lasers. *OPN Optics in 2016*, December-2016.

BIBLIOGRAPHY

1 SIEGMAN, A. E. *Lasers*. 1. ed. Mill Valey, CA. USA: University Science Books, 1986. v. 1. ISBN 0-935702-11-5.

2 DAINTY, J. C. *Laser Speckle and Related Phenomena (Topics in Applied Physics 9).* New York: [s.n.], 1975.

3 SOEST, G. V.; POELWIJK, F. J.; LAGENDIJK, A. Speckle experiments in random lasers. *Physical Review E*, American Physical Society, v. 65, p. 046603, Mar 2002.

4 ROCHA, M. N. et al. O azul do céu e o vermelho do pôr-do-sol. *RBEF*, v. 32, n. 3, p. 3501–1–3501–3, 2010.

5 HULBURT, E. O. Explanation of the brightness and color of the sky, particularly the twilight sky. *J. Opt. Soc. Am.*, OSA, v. 43, n. 2, p. 113–118, Feb 1953.

6 SAKURADA, Y.; NAKAMURA, T. Demonstration of the light scattering phenomenon in the atmosphere. *Seventh International Conference on Education and Training in Optics and Photonics, Proceedings of SPIE.*, v. 4588, 2002.

7 CHU, B. *Laser light scattering.*: Basic principles and practice. 2. ed. State University of New York, New York: [s.n.], 1991.

8 CAO, H. Lasing in random media. *Waves in Random Media*, v. 13, n. 3, p. R1–R39, 2003.

9 LAWANDY, N. M. et al. Laser action in strongly scattering media. *Letters to nature*, v. 368, p. 436–438, 1994.

10 TURITSYN, S. K. et al. Random distributed feedback fibre lasers. *Physics Reports*, v. 542, n. 2, p. 133 – 193, 2014. ISSN 0370-1573. Random Distributed Feedback Fibre Lasers.

11 SANTOS., M. V. dos et al. Random laser action from flexible biocellulose-based device. *Journal of Applied Physics*, v. 115, n. 8, p. 083108, 2014.

12 CAO, H. et al. Ultraviolet lasing in resonators formed by scattering in semiconductor polycrystalline films. *Applied Physics Letters*, v. 73, n. 25, p. 3656–3658, 1989.

13 LETOKHOV, V. S. Generation of Light by a Scattering Medium with Negative Resonance Absorption. *Soviet Journal of Experimental and Theoretical Physics*, v. 26, p. 835, april 1968.

14 AMBARTSUMYAN, R. V.; KRYUKOV, P. G.; LETOKHOV, V. C. Dynamics of emission line narrowing for a laser with nonresonant feedback. *Soviet Journal of Experimental and Theoretical Physics*, v. 24, n. 6, p. 1129–1134, June 1967.

15 AMBARTSUMYAN, R. V. et al. A laser with nonresonant feedback. *Soviet Journal of Experimental and Theoretical Physics*, v. 24, n. 3, p. 481–485, March 1967.

16 AMBARTSUMYAN, R. V. et al. Statistical emission properties of a nonresonant feedback laser. *Soviet Journal of Experimental and Theoretical Physics*, v. 26, n. 6, p. 1109–1114, June 1968.

17 AMBARTSUMYAN, R. V. et al. Emission spectrum of an He-Xe laser with nonresonant feedback. *Soviet Journal of Experimental and Theoretical Physics*, v. 31, n. 2, p. 234–241, August 1970.

18 CAO, H. et al. Random laser action in semiconductor powder. *Physical Review Letters*, v. 82, n. 11, p. 2278–2281, 1999.

19 SHA, W. L.; LIU, C.-H.; ALFANO, R. R. Spectral and temporal measurements of laser action of rhodamine 640 dye in strongly scattering media. *Optics Letters*, v. 19, p. 1922–1924, 1994.

20 SHI, X. et al. Dissolvable and recyclable random lasers. *ACS Nano*, v. 11, n. 8, p. 7600 – 7607, 2017.

21 POLSON, R. C.; VARDENYA, Z. V. Random lasing in human tissues. *Applied Physics Letters*, v. 85, n. 1289, p. 1289–1291, 2004.

22 MATOS, C. J. S. de et al. Random fiber laser. *Phys. Rev. Lett.*, American Physical Society, v. 99, p. 153903, Oct 2007.

23 TURITSYN, S. K. et al. Random distributed feedback fibre lasers. *Nature Photonics*, v. 542, n. 2, p. 133 – 193, 2014. ISSN 0370-1573. Random Distributed Feedback Fibre Lasers.

24 WIERSMA, D. S. The physics and applications of random lasers. *Nature Physics*, v. 4, p. 359–367, May 2008.

25 REDDING, B.; CHOMA, M. A.; CAO, H. Speckle-free laser imaging using random laser illumination. *Nature Photonics*, v. 5, n. 355, p. 355–359, 2012.

26 DÄNDLIKER, R. Concept of modes in optics and photonics. *Proc SPIE*, p. 193–198, 06 2000.

27 CAO, H. Review on latest developments in random lasers with coherent feedback. *Review on latest developments in random lasers with coherent feedback*, v. 38, n. 10497, p. 10497–10535, 2005.

28 UPPU, R.; TIWARI, A. K.; MUJUMDAR, S. Identification of statistical regimes and crossovers in coherent random laser emission. *Optics Letters*, v. 37, n. 04, p. 662–664, 2012.

29 UPPU, R.; MUJUMDAR, S. Exponentially tempered lévy sums in random lasers. *Physical Review Letters*, v. 114, n. 183903, p. 1–5, 2015.

30 LUAN, F. et al. Lasing in nanocomposite random media. *NanoToday*, Science Direct, v. 10, p. 168–192, 2015.

31 TENOPALA-CARMONA, F. et al. Angular distribution of random laser emission. *Optics Letters*, v. 39, n. 3, 2014.

32 SZNITKO, L.; MYSLIWIEC, J.; MINIEWICZ, A. The role of polymers in random lasing. *Journal of Polymer Science Part B: Polymer Physics*, v. 53, n. 14, p. 951–974, 2015.

33 HISCH, T. et al. Pump-controlled directional light emission from random lasers. *Phys. Rev. Lett.*, American Physical Society, v. 111, p. 023902, Jul 2013.

34 WIERSMA, D. S. Clear directions for random lasers. *Nature*, Nature Publishing Group, v. 111, p. 023902, Jul 2013.

35 UPPU, R.; MUJUMDAR, S. Lévy exponents as universal identifiers of threshold and criticality in random lasers. *Physical Review A*, v. 90, n. 025801, p. 1–5, 2012.

36 CAO, H. et al. Random lasers with coherent feedback. *IEEE journal of selected topics in quantum electronics*, v. 09, n. 1, 2003.

37 GHOFRANIHA, N. et al. Experimental evidence of replica symmetry breaking in random lasers. *Nature Communications*, v. 6, n. 6058, 2015.

38 ANTENUCCI, F.; CRISANTI, A.; LEUZZI, L. The glassy random laser: replica symmetry breaking in the intensity fluctuations of emission spectra. *Scientific Reports*, v. 5, 2015.

39 MARKUSHEV, V. M.; ZOLIN, V. F.; BRISKINA, C. M. Luminescence and stimulated emission of neodymium in sodium lanthanum molybdate powders. *Soviet Journal of Quantum Electronics [BRIEF COMMUNICATION]*, v. 16, n. 2, p. 281–282, 1986.

40 GOMES, A. S. L. et al. Observation of lévy distribution and replica symmetry breaking in random lasers from a single set of measurements. *Scientific Reports*, v. 6, n. 27987, p. 1–8, 2016.

41 CARREÑO, S. J. et al. Interplay between random laser performance and self-frequency conversions in $\mathrm{nd}_x\mathrm{y}_{1.00-x}\mathrm{al}_3(\mathrm{bo}_3)_4$ nanocrystals powders. *Optical Materials*, Nature Publishing Group, v. 54, p. 262–268, 2016.

42 WIERSMAN, D. S.; ALBADA, M. P. van; LAGENDIJK, A. Reply to random laser? scientific correspondence. *Nature*, v. 373, p. 203–204, 1995.

43 LAWANDY, N. M. et al. Reply to random laser? scientific correspondence. *Nature*, v. 373, p. 204–204, 1995.

44 ZHU, G.; GU, L.; NOGINOV, M. A. Experimental study of instability in a random laser with immobile scatterers. *Physical Review A*, v. 85, n. 04381, p. 1–5, 2012.

45 PINCHEIRA, P. I. R. et al. Observation of photonic paramagnetic to spin-glass transition in a specially designed tio2 particle-based dye-colloidal random laser. *Opt. Lett.*, OSA, v. 41, n. 15, p. 3459–3462, Aug 2016.

46 CHURKIN, D. V. et al. Recent advances in fundamentals and applications of random fiber lasers. *Adv. Opt. Photon.*, OSA, v. 7, n. 3, p. 516–569, Sep 2015.

47 POPP, J.; KIEFER, W. *Raman scattering, fundamentals*. [S.l.]: Encyclopeida of analytical Chemistry, 2006.

48 HOKR, B. H. et al. Bright emission from a random raman laser. *Nature Communications*, v. 5, n. 4351, 2014.

49 GAGNÉ, M.; KASHYAP, R. Demonstration of a 3 mw threshold er-doped random fiber laser based on a unique fiber bragg grating. *Optics Express*, v. 17, n. 21, p. 19067–19074, 2009.

50 SAVAGE, N. Identifying explosives at a distance. *IEEE Spectrum*, v. 51, n. 10, 2014.

51 ZHANG, H. et al. More than 400 w random fiber laser with excellent beam quality. *Opt. Lett.*, OSA, v. 42, n. 17, p. 3347–3350, Sep 2017.

52 GAGNÉ, M.; KASHYAP, R. Random fiber bragg grating raman fiber laser. *Opt. Lett.*, OSA, v. 39, n. 9, p. 2755–2758, May 2014.

53 KASHYAP, R. *Spin Glasses and Complexity*: Primers in complex systems. 2. ed. [S.l.]: Elsevier. Academic Press 2010, 2009. v. 1. ISBN 9780080919911.

54 AGRAWAL, G. P.; RADIC, S. Phase-shifted fiber bragg gratings and their application for wavelength demultiplexing. *IEEE Photonics Technology Letters*, v. 6, n. 8, p. 995–997, Aug 1994. ISSN 1041-1135.

55 LIZÁRRAGA, N. et al. Single-mode Er-doped fiber random laser with distributed Bragg grating feedback. *Optics Express*, v. 17, n. 2, p. 395–404, 2009.

56 GAGNÉ, M. et al. Novel custom fiber bragg grating fabrication technique based on push-pull phase shifting interferometry. *Optics Express*, v. 16, n. 26, p. 21550–21557, 2008.

57 GAGNÉ, M. et al. Fabrication of high quality, ultra-long fiber bragg gratings: up to 2 million periods in phase. *Opt. Express*, OSA, v. 22, n. 1, p. 387–398, Jan 2014.

58 GOMES, A. S. L. et al. Glassy behavior in a one-dimensional continuous-wave erbium-doped random fiber laser. *Physical Review A*, v. 94, 07 2016.

59 DOTSENKO, V. *Introduction to the Theory of Spin Glasses and Neural Networks*. River Edge, NJ, USA: World Scientific Publishing Company, 1994. (World Scientific Lecture Notes in Physics). ISBN 9789810218737.

60 MEGARD, M.; PARISI, G.; VIRASOO, M. A. *Spin glass theory and beyond*. 1. ed. [S.l.]: World Scientific, 1987. v. 9. (World Scientific lecture notes in physics 9, v. 9). ISBN 9971501155,9789971501150,9971501163,9789971501167.

61 STEIN, D. L.; NEWMAN, C. M. *Spin Glasses and Complexity*: Primers in complex systems. 1. ed. 41 William Street, Princeton New Jersey 08540: Princeton University Press, 2013. v. 4. ISBN 978-0-691-14733-8.

62 BINDER, K.; YOUNG, A. P. Spin glasses: Experimental facts, theoretical concepts, and open questions. *Reviews of Modern Physics*, v. 58, n. 4, p. 801 – 976, 1986.

63 BRUSH, S. G. History of the lenz-ising model. *Reviews of Modern Physics*, v. 39, n. 4, p. 883, 1967.

64 ANTENUCCI, F. et al. Statistical mechanics models for multimode lasers and random lasers. *Philosophical Magazine*, v. 96, 09 2015.

65 ANGELANI, L. et al. Glassy behavior of light. *Phys. Rev. Lett.*, American Physical Society, v. 96, p. 065702, Feb 2006.

66 ANGLOS, D. et al. Random laser action in organic–inorganic nanocomposites. *J. Opt. Soc. Am. B*, v. 21, n. 01, p. 208–213, 2004.

67 SHARMA, D.; RAMACHANDRAN, H.; KUMAR, N. Lévy statistical fluctuations from a random amplifying medium. *Fluctuation and Noise Letters*, v. 06, n. 01, p. L95–L101, 2006.

68 IGNESTI, E. et al. Experimental and theoretical investigation of statistical regimes in random laser emission. *Physical Review A*, v. 88, n. 033820, p. 1–7, 2013.

69 STOCHASTIC Process with Ultraslow Convergence to a Gaussian: The Truncated Levy Flight. *Physical Review Letters*, v. 73, n. 22, p. 2946–2949, 1994.

70 BARNDORFF-NIELSENSIDNEY, O. E.; RESNICK, I.; MIKOSCH, T. *Lévy Processes*: Theory and applications. Birkhäuser Boston 2001: [s.n.], 2001.

71 VISWANATHAN, G. M. et al. Lévy flight search patterns of wandering albatrosses. *Nature*, v. 381, p. 413–415, 1996.

72 VISWANATHAN, G. M. et al. *The Physics of Foraging*: An introduction to random searches and biological encounters. Cambridge, UK: Cambridge University Press, 2011.

73 EMBRECHTS, P.; KLUPPELBERG, C.; MIKOSCH, T. *Modelling Extremal Events: for Insurance and Finance (Stochastic Modelling and Applied Probability)*. 1. ed. [S.l.]: Springer-Verlag Berlin Heidelberg, 2008. ISBN 9783540609315.

74 JONES, E. et al. *SciPy: Open source scientific tools for Python*. 2001–. [Online; accessed April 25, 2019http://www.scipy.org/].

75 LEPRI, S. et al. Statistical regimes of random laser fluctuations. *Physical Review A*, v. 75, n. 063820, p. 1–7, 2007.

76 RAPOSO, E. P.; GOMES, A. S. L. Analytical solution for the lévy-like steady-state distribution of intensities in random lasers. *Phys. Rev. A*, American Physical Society, v. 91, p. 043827, Apr 2015.

77 ZAITSEV, O.; DEYCH, L.; SHUVAYEV, V. Statistical properties of one-dimensional random lasers. *Phys. Rev. Lett.*, American Physical Society, v. 102, p. 043906, Jan 2009.

78 LIMA, B. C. et al. Observation of lévy statistics in one-dimensional erbium-based random fiber laser. *J. Opt. Soc. Am. B*, OSA, v. 34, n. 2, p. 293–299, Feb 2017.

79 MCCULLOCH, J. H. Simple consistent estimators of stable distribution parameters. *Communications in Statistics. Simulation and Computation*, Taylor and Francis, v. 15, n. 4, p. 1109–1136, 1986.

80 SCIPY v1.2.0 Reference Guide. 2001–.

81 SORNETTE, D. *Critical Phenomena in Natural Sciences*: Chaos, fractals, selforganization and disorder: Concepts and tools. [S.l.]: Springer-Verlag Berlin Heidelberg, 2006. ISBN 978-3-540-33182-7.

82 BITNER-GREGERSEN, E. *Rethinking Rogue Waves: Towards better modelling, insight and action*. 2006. [Online; accessed April 25, 2019https://www.dnvgl.com/feature/rogue-waves.html].

83 BROAD, W. J. *Rogue Giants at sea*. The new york times. [Online; accessed April 25, 2019https://www.nytimes.com/2006/07/11/science/11wave.html].

84 MOLONEY, N. R.; DAVIDSEN, J. Extreme value statistics in the solar wind: An application to correlated lévy processes. *Journal of Geophysical Research*, v. 115, n. A10114, p. 1–9, 2010.

85 SOLLI, D. R. et al. Optical rogue waves. *Nature*, Nature Publishing Group, v. 450, n. 1054, Dec. 2012.

86 DUDLEY, J. M.; GENTY, G.; EGGLETON, B. J. Harnessing and control of optical rogue waves in supercontinuum generation. *Opt. Express*, OSA, v. 16, n. 6, p. 3644–3651, Mar 2008.

87 HAMMANI, K. et al. Optical rogue-wave-like extreme value fluctuations in fiber raman amplifiers. *Opt. Express*, OSA, v. 16, n. 21, p. 16467–16474, Oct 2008.

88 HAMMANI, K.; FINOT, C.; MILLOT, G. Emergence of extreme events in fiber-based parametric processes driven by a partially incoherent pump wave. *Opt. Lett.*, OSA, v. 34, n. 8, p. 1138–1140, Apr 2009.

89 GORBUNOV, O. A.; SUGAVANAM, S.; CHURKIN, D. V. Intensity dynamics and statistical properties of random distributed feedback fiber laser. *Opt. Lett.*, OSA, v. 40, n. 8, p. 1783–1786, Apr 2015.

90 UPPU, R.; MUJUMDAR, S. Extreme value statistics of intensity fluctuations in random lasers. In: *Frontiers in Optics 2015*. [S.l.]: Optical Society of America, 2015. p. FTh1G.5.

91 LIMA, B. C. et al. Extreme-value statistics of intensities in a cw-pumped random fiber laser. *Phys. Rev. A*, American Physical Society, v. 96, p. 013834, Jul 2017.

92 TOMMASI, F. et al. Statistical outliers in random laser emission. *Phys. Rev. A*, American Physical Society, v. 98, p. 053816, Nov 2018.

93 LIMA, B. C. et al. Fluctuations statistics in an erbium random fiber laser. In: *Frontiers in Optics / Laser Science*. [S.l.]: Optical Society of America, 2018. p. JW3A.73.

94 GONZÁLEZ, I. R. et al. Coexistence of turbulence-like and glassy behaviours in a photonic system. *Scientific Reports*, v. 8, 11 2018.

95 Gao, S. et al. High-speed random bit generation via brillouin random fiber laser with non-uniform fibers. *IEEE Photonics Technology Letters*, v. 29, n. 16, p. 1352–1355, 2017.

96 XIANG, D. et al. Truly random bit generation based on a novel random brillouin fiber laser. *Opt. Lett.*, OSA, v. 40, n. 22, p. 5415–5418, Nov 2015.